SOURCE, TRANSPORT, AND EVOLUTION OF SALINE GROUNDWATER IN A SHALLOW HOLOCENE AQUIFER ON THE TIDAL DELTAPLAIN OF SOUTHWEST BANGLADESH

By

Scott C. Worland

Submitted to the Faculty of the

Graduate School of Vanderbilt University

in partial of the requirements

for the degree of

MASTER OF SCIENCE

in

Earth and Environmental Sciences

August, 2014

Nashville, Tennessee

Approved By:

George M. Hornberger

Steven L. Goodbred

To the people of Bangladesh

ACKNOWLEDGMENTS

It has become difficult to attribute specific thoughts to specific places, so I formally thank all those upstream. Special thanks to my advisor and mentor, Dr. George Hornberger, for making the "existence, origin, movement, and course of waters and the causes which govern and direct their movement," less "secret, occult, and concealed" (*Ohio-Supreme-Court*, 1861). Other EES faculty who have given me considerable help, including Dr. David Furbish, Dr. Steve Goodbred, Dr. John Ayers, Dr. Jonathan Gilligan, and Dr. Jessica Oster. The Office of Naval Research for funding this research. My research group for tripling as a scrupulous editorial board, a book club and a food network. My fellow graduate students, Tyler Doane–for his willingness to sharpen my mathematics and helping me discover seven things that just must be so, and Christopher Myers–for his binary roles: a surreptitious-disassembler of my office chair and an always thoughtful peer reviewer. The Bangladesh team, specifically Carol Wilson, David Fry, and Zitu. I thank Antonio Lucio Vivaldi, for writing the music that has been a close companion these last two years. I thank my parents for making me play outside. I thank my 20 month old daughter, NoraJean (and the stork that delivered her), for her silliness that always decreases my cortisol levels and reminds me of what is important. Lastly, and most importantly, I thank my wife, Bonnie Worland, for her normally-only-found-in-fairytale: love, support, forgiveness, understanding, trust, encouragement, patience, and guidance.

Table of Contents

List of Tables

List of Figures

Chapter I

INTRODUCTION

Riverine deltas and their adjacent coastal plains host 500 million people (*Small and Nicholls*, 2003). Deltas are dynamic natural and socio-economic environments that are sensitive to the effects of urbanization, natural disasters and sea level change. Many of the worlds megacities are located on fragile delta systems, such as Dhaka, Kolkata, Shanghai, and Bangkok, and projections estimate increasing delta inhabitation with a growing global population *Small and Nicholls* (2003); *Syvitski et al.* (2009). Densely populated areas generate increased stress on water availability. Deltaic groundwater resources are often vulnerable to degradation from seawater intrusion or through interaction with saline paleowaters (*Tran*, 2012). High salinity groundwaters can extend hundreds of kilometers inland from the coast, severely restricting the use of groundwater for sanitation, drinking and irrigation (*Wang et al.*, 2013; *Tran*, 2012; *Bahar and Reza*, 2010). Where the supply of freshwater is not adequate, the forced consumption of saline water can impact health by promoting the development of renal failure, kidney disease, hypertension and gastrointestinal irritation (*Davis and DeWiest*, 1966; *Plunkett*, 1976; *Khan et al.*, 2011).

This study of saline groundwaters is located in Bangladesh, on the Ganges-Brahmaputra-Meghna (GBM) River delta, the largest and most densely populated delta system in the world. The GBM deltaic plains sustain rich fisheries and agriculture, which support a pop-

ulation of 160 million people, giving Bangladesh one of the highest population densities in the world. For water resources, these people have traditionally used surface water that is often laden with pathogens. In an attempt to reduce disease stemming from polluted surface water, millions of tube wells were drilled to extract the shallow groundwater at the end of the twentieth century. In many places though, the shallow groundwater is contaminated with arsenic as anoxic conditions within the aquifer permitted the reductive dissolution of ferric oxyhydroxides and, consequently, the mobilization of arsenic (*Alam et al.*, 2002; *McArthur et al.*, 2001). Arsenic concentrations 200 times greater than the World Health Organization guideline for drinking water motivated extensive studies on the geochemical controls of arsenic release and the characterization of the hydrogeology in Bangladesh (*Michael and Voss*, 2009; *Ravenscroft et al.*, 2005; *Bahar and Reza*, 2010).

The Bengal basin is bounded by the Himalayas and the Shillong Plateau to the north, the Indian craton to the west and the Indo-Burman ranges to the east (*Morgan and McIntire*, 1959). The massive Holocene floodplains consist of poorly developed, immature silt and clay soils that are underlain by Himalayan derived sediments deposited since the Pliocene (*Alam et al.*, 1990; *Ravenscroft et al.*, 2005; *Morgan and McIntire*, 1959). On a national scale, the simplified hydrogeology is represented by two distinct aquifers vertically separated by Pleistocene clays (*MPO*, 1987). The basin is often treated as homogenous and isotropic, but is more accurately represented as zonally homogenous and partitioned by hydrogeologic properties that describe the heterogeneity of each region (*Michael and Voss*, 2009). *Ravenscroft et al.* (2005) proposed three groundwater flow systems that operate simultaneously

on different scales: (1) local topographic constrained flow over a distance of a few kilometers and several meters to tens of meters deep, (2) an intermediate flow system between regionally prominent topographic features with flow paths tens of kilometers long, extensive residence times of hundreds to thousands of years and operating depths of one to several hundred meters deep, and (3) a basin-scale flow system with gradient driven flow from the basin boundaries to the coast, residence times of tens of thousands of years and operating depths of more than two hundred meters.

1.1 Motivation

Although arsenic in groundwater is a serious issue in many areas of the GBM delta, high salinity also affects the adequacy of the water supply and further complicates drinking water issues on the lower delta plain. It is estimated that twenty million coastal inhabitants in Bangladesh are directly affected by saline drinking water (*Khan et al.*, 2011). In rural areas, many tubewells are drilled to depths less than 50 meters, and these shallow wells produce water of varying salinity. In the Southwest region, the salinity of the shallow aquifers (<100 meters) generally increases from north to south, although there are pockets of fresh or modestly saline water in the more saline portions of the shallow aquifer (*Yu et al.*, 2010; *WARPO*, 2008–2009; *Bahar and Reza*, 2010; *George*, 2013). Initially, the brackish groundwater in the coastal regions of Bangladesh was thought to originate from modern seawater through tidal channel mixing, flood inundation, and seawater intrusion and this hypothesis is frequently cited as the source of shallow and deep groundwater salinity (*Alam*, 1996; *Khan*

et al., 2011; *MPO*, 1987; *Bahar and Reza*, 2010; *Zahid et al.*, 2008; *Hoque et al.*, 2003a). Although seawater intrusion may explain deep aquifer salinity, it is an unlikely explanation of shallow groundwater salinity hundreds of kilometers inland from the coast (*Delsman et al.*, 2013; *Michael et al.*, 2013). *Tasich and Hornberger* (2012) demonstrated that surface water–groundwater interactions are minimal due to the low permeability of the tidal channel banks and *George* (2013) showed that groundwater salinity is not correlated with areas of flood inundation. We hypothesize that the shallow brackish water is paleo-seawater deposited within the early holocene. During the construction of the tide-influenced-lower deltaplain, saline porewaters were co-deposited along with the sediments that form the shallow aquifer (*Delsman et al.*, 2013; *Hoque et al.*, 2003a; *Goodbred and Kuehl*, 2000).

1.2 Research Questions

The research questions for the study are:

1. Is the shallow (less than 100 m) groundwater modern or connate (water trapped in pores during deposition)?
   (a) Is modern seawater influence a likely explanation of salinity?
   (b) Can the shallow aquifer salinity be explained by the mixing of paleo-seawater and fresh meteoric water?
2. What controls the salinity distribution?
   (a) Does the variable thickness of the surface confining unit allow isolated pockets of direct recharge?

Chapter II

METHODS

This study employs a combination of ^{3}H and ^{14}C dating, electromagnetic (EM) subsurface mapping, and a 2D solute transport model and focused on the smallest hydrogeological scale presented above by *Ravenscroft et al.* (2005).

2.1 Study Site: Polder 32

In the 1960s Bangladesh began promoting the use of polders to expand and develop rice production in delta lowlands (*Brammer*, 1983; *Hoque et al.*, 2003b). A polder is a section of low-lying land that has been reclaimed from marine or alluvial environments and protected by embankments. The shallow groundwater beneath polders in the southwest region of the country is primarily brackish (∼5 g/l) with isolated instances where much fresher (<1.5 g/l) water can be found (Figure 2.1). A small scale hydrologic investigation of groundwater salinity beneath a 60 km^2 polder, Polder 32 (polder numbers generated by the Bangladesh Water Development Board), located in southwest Bangladesh was undertaken to explore possible hydrogeological explanations of the distribution of water salinities in the shallow aquifer. Polder 32 is located in the Ganges Delta, in the Dacope Upazila, 90 km inland from the Bay of Bengal and 30 km southwest of the city of Khulna (Figure 2.1). A formerly forested mangrove system, the polder is hedged by tidal channels that are former distributaries of the

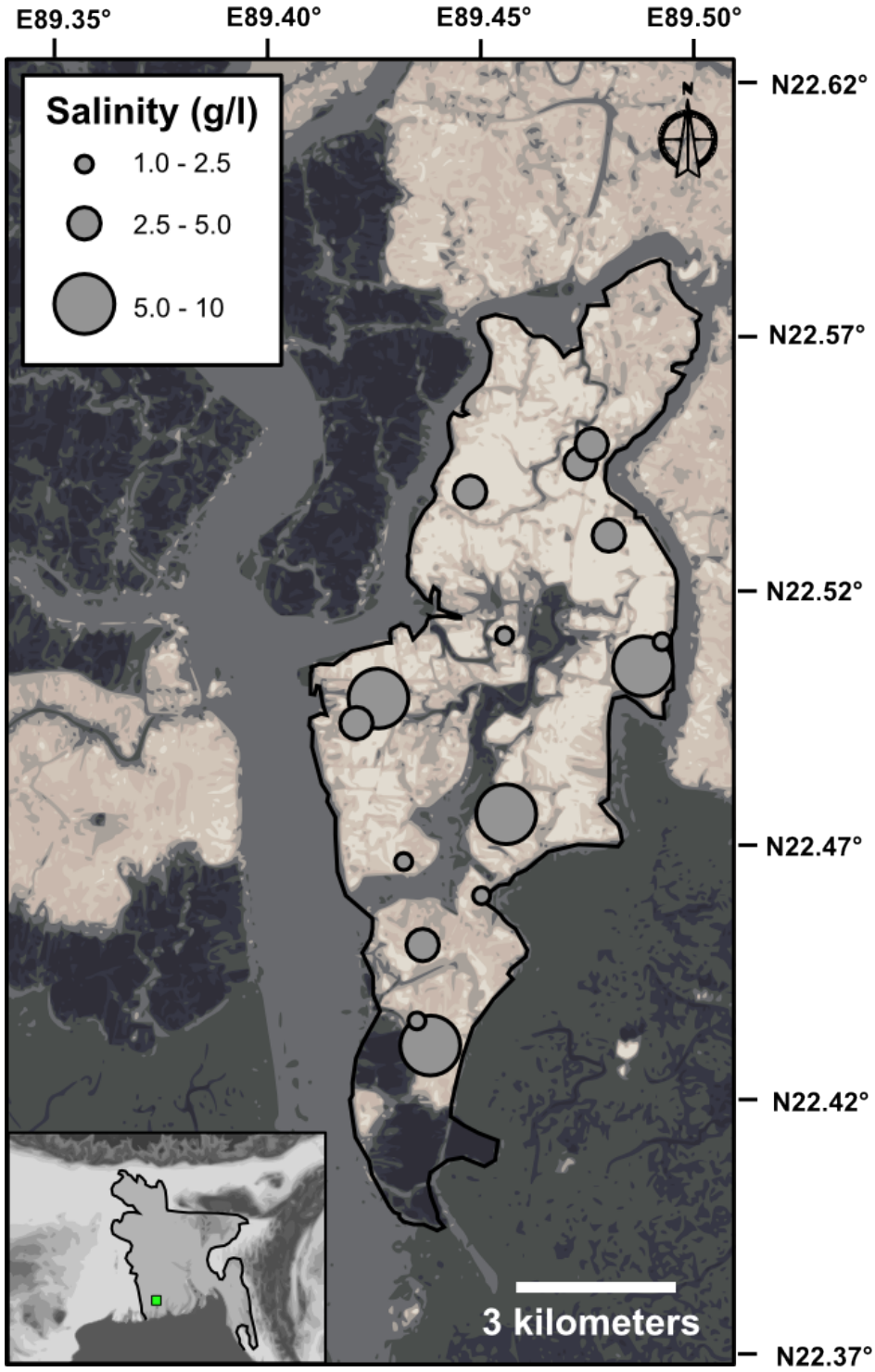

Figure 2.1: Study site, Polder 32 in Southwest Bangladesh, with variable tubewell salinity (*George*, 2013).

Ganges River. Its lower half lies adjacent to a protected mangrove forest while its upper half is surrounded by other polders and agricultural land. Sediment data collected on the polder reveals a mud confining unit underlain primarily by sands with small mud units throughout (figure 2.2). The hydrogeology of the Khulna region has been generally described as a three aquifer system consisting of a semi-confined, shallow Holocene aquifer extending 100 meters below ground level (bgl) that is vertically separated from two Pleistocene aquifers, which extend 200 and 300 meters bgl (*Rahman et al.*, 2011b; *Burgess et al.*, 2010). The local economy is supported primarily by mixed rice cultivations and shrimp aquaculture. A recent survey taken on Polder 32 indicates that almost three quarters of the polder residents use shallow groundwater as their main source of drinking water for at least some portion of the year (Laura Benneyworth, personal communication). During the dry season, the livelihood of polder communities are dependent on access to fresh water, and members of households periodically walk over two kilometers to gather water from less saline wells.

2.2 Isotopes

2.2.1 Sample Collection

Water was collected from five pre-existing tubewells (depths of 20-50 meters, Figure 2.2) located on the polder, including a monitoring well located at a Managed Artificial Recharge (MAR) site (Figure 2.3). The wells were chosen based on knowledge of regional flow from the northwest to southeast. The wells were purged one well volume prior to sampling. The sample bottles were rinsed thoroughly with formation water prior to collecting the samples.

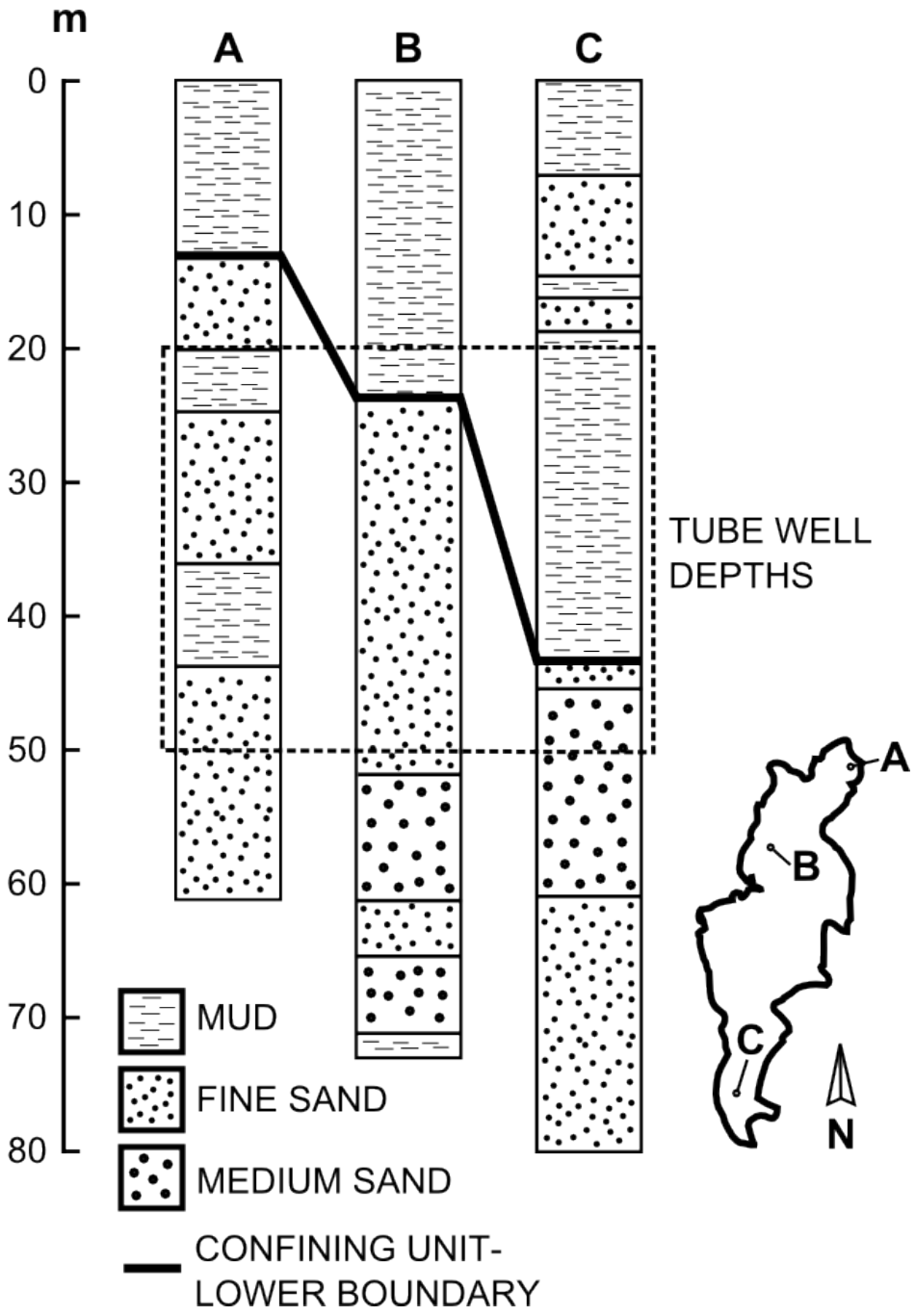

Figure 2.2: Figure based on sediment core data collected on Polder 32 by Wilson et al., 2013.

In order to reduce interaction with the atmosphere, the well heads were removed and a peristaltic pump was used to extract the water and fill the sample containers. The water samples for Carbon-14 (^{14}C) analysis were collected in 1-L Nalgene plastic bottles and the samples were pre-treated with one gram of NaOH to fix carbonate species within the sample. The water samples for tritium (^{3}H) analysis were collected in 0.5-L glass bottles. All bottles were sealed with tape to ensure no interaction with the atmosphere.

2.2.2 Laboratory Methods

Dissolved inorganic carbon (DIC) was analyzed using accelerated mass spectrometry at Geochron Laboratories, Chelmsford, MA. Tritium analysis was conducted at the Dissolved and Noble Gas Lab, University of Utah, using helium ingrowth, a technique pioneered by *Cook and Solomon* (1997). High concentrations of tritium were added to the atmosphere in the mid twentieth century as the result of thermonuclear testing. This allows tritium to be used a historical, slug-like tracer and is indicative of the influence of modern water.

2.2.3 Correction for Carbon-14 Dates

Raw radiocarbon dates were calculated using the following equation,

$$^{14}\mathrm{C}_{\mathrm{age(yrs)}} = \frac{1}{-\lambda} * \ln(\frac{^{14}\mathrm{Cpm}}{100}), \tag{2.1}$$

where $^{14}C_{pm}$ is the percent modern DIC in the groundwater, and λ is 8035 years, the half life of ^{14}C divided by the ln(2). The raw dates were then calibrated using the OxCal software, *Bronk* (2013); *Ramsey* (2009), which uses the most recent calibration curve, IntCal-13, generated by *Reimer et al.* (2013).

The correction model is taken from a previous groundwater investigation in Bangladesh completed by *Hoque and Burgess* (2012). ^{14}C and ^{3}H data were compiled to estimate the initial activity of ^{14}C and 87 percent modern was used to correct the raw radiocarbon dates (figure 3.1) (*Hoque and Burgess*, 2012; *Geyh et al.*, 2000). The dates were calculated using the following equation,

$$^{14}C_{age(yrs)} = \frac{1}{-\lambda} * \ln(\frac{^{14}C_{pm}}{87}), \tag{2.2}$$

The corrected ages were then calibrated using the OxCal software.

2.3 Electromagnetic Induction

EM surveys have been shown to provide useful insights to grain size distribution and porosity estimations (*Evans et al.*, 2001; *Triantafilis and Lesch*, 2005; *Smith and Sjogren*, 2006). A Geophex GEM-2 handheld, multi-frequency terrain conductivity meter was used to investigate the EM response of the shallow subsurface. Multiple transects were taken laterally on the polder while recording transmission frequencies of 1530 Hz, 5310 Hz, and 63030 Hz (Figure 2.3). These frequencies were chosen because their range allows EM analysis of different depths. The GEM-2 was operated in a horizontal coplanar orientation 1 meter above the ground surface. A GPS was used to determine points along the transect and line-of-sight

was used to traverse the landscape. The inphase and quadrature data were converted into apparent conductivity using a conductive and magnetic half-space model by an application in the *Aeroquest* software (*Huang and Won*, 2000). The 1-D inversion model was created using the University of British Columbia Geophysical Inversion facility (UBC-GIF) EM1DFM inversion program. The program constructs 1-D models for frequency-domain EM data (*Farquharson*, 2000). The inphase and quadrature observations were presented in parts per million, and an electrical conductivity model was created (with fixed magnetic susceptibility). Each sounding from the transect is interpreted independently, and a composite 2-D model is created. The starting conductivity model file consisted of eight equally spaced layers with a basement half-space below 20 meters. The inversion trade-off parameter was automatically chosen using the generalized cross-validation criterion. The EM1DFM output was scanned with eight color bands to smooth the data. Areas of high background noise and model artifacts were smoothed to a greater extent. The smoothing process did not change the model structure.

2.4 Finite Element Model

The 2-D finite element mesh was generated using *DistMesh*, a mesh generator for MATLAB (*Persson and Strang*, 2004). A relatively coarse mesh was chosen as the modelling is an exploratory analysis. The model depicts the numerical solution of the advection-dispersion

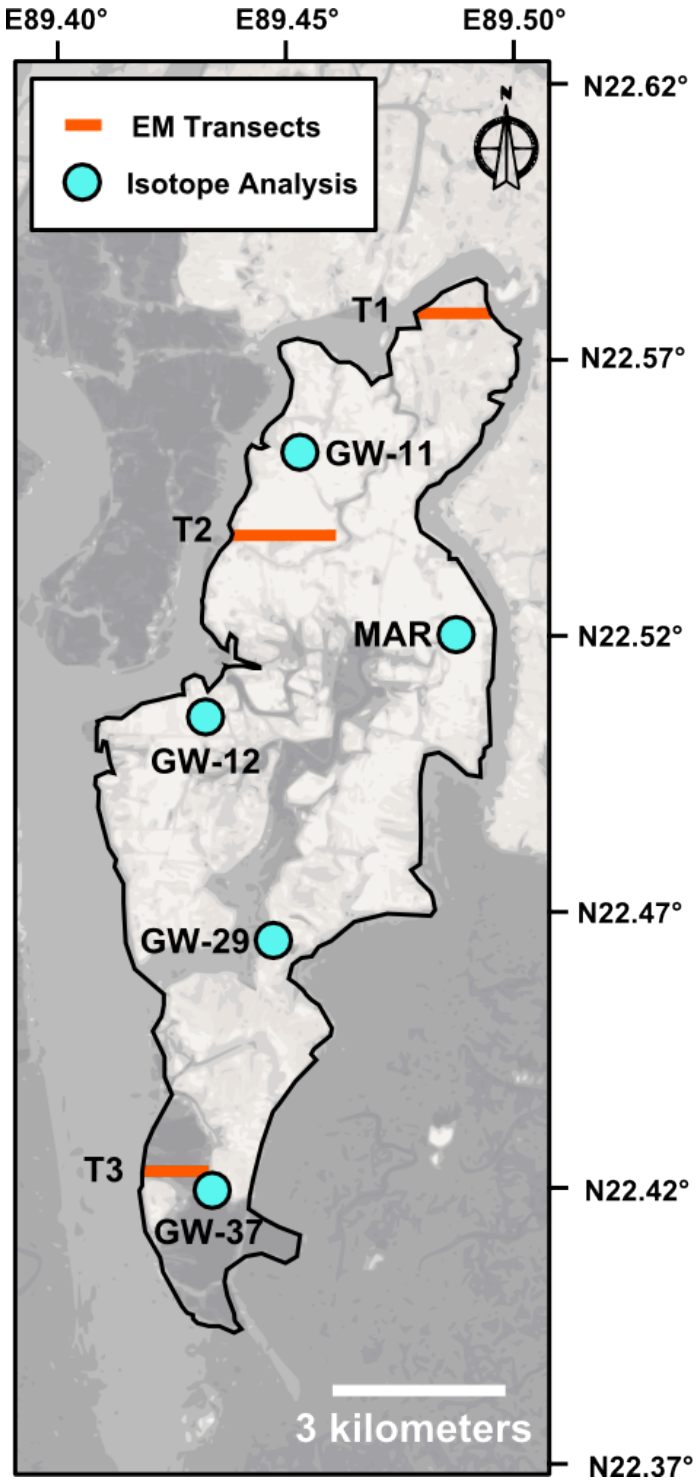

Figure 2.3: Tube well, sediment core and EM transect locations

equation (ADE),

$$\frac{\partial c}{\partial t} = -u_x \frac{\partial c}{\partial x} - u_y \frac{\partial c}{\partial y} + [D^* + D_x] \frac{\partial^2 c}{\partial x^2} + [D^* + D_y] \frac{\partial^2 c}{\partial y^2} + \gamma, \tag{2.3}$$

where $\frac{\partial c}{\partial t}$ is the change in salt concentration over time, u_x and u_y are the advection terms and $[D^* + D_x]$ and $[D^* + D_y]$ are the hydrodynamic dispersion coefficients, where D^* is the molecular diffusion coefficient and D_x and D_y are the mechanical dispersion terms. The advection terms in Equation 3 are calculated by numerically solving the groundwater flow equation over the mesh using fixed head boundary conditions,

$$\frac{\partial}{\partial x}\left(T\frac{\partial h}{\partial x}\right) + \frac{\partial}{\partial y}\left(T\frac{\partial h}{\partial y}\right) + R = 0, \tag{2.4}$$

where T is the transmissivity and $\frac{\partial h}{\partial x}$ is the change in hydraulic head in the x direction, $\frac{\partial h}{\partial y}$ in the y direction and R [Lt^{-1}] is local recharge which was added to select elements to represent possible localized pathways through the clay cap. Two different T scenarios were used in the model, (1) isotropic and T and (2) anisotropic T where 300 elements were randomly selected to be assigned a smaller T value (table II.1). The equations were implicitly solved and weighted using the Galerkin weighted residual method.

2.4.1 Boundary Conditions

Dirichlet and Neumann boundary conditions were implemented in the model (Figure 2.4). The northernmost boundary is a fixed head boundary condition and an advective flux solute transport boundary condition. The boundaries along the side of the model are zero flux boundaries. The two southern most boundaries were fixed head boundary and flux boundaries involving only advection. The velocity component normal to the boundary elements was calculated using a time step of one year. The calculated normal velocities were multiplied by concentration, element length, and aquifer depth to obtain a mass flux at the specified boundaries. The model was initialized with a salinity of 6.3 g/l, which is the current annual mean of the salinities in the tidal channels surrounding the polder (*Auerbach*, 2013). Time zero in the model was informed by the isotope results, and was set to 6000 YBP.

2.4.2 Direct Recharge Elements

Direct recharge refers to meteoric water that falls on the surface and infiltrates into the shallow aquifer. Direct recharge was included in both the flow and transport equations at selected elements by using the source terms in Equations 3 and 4.

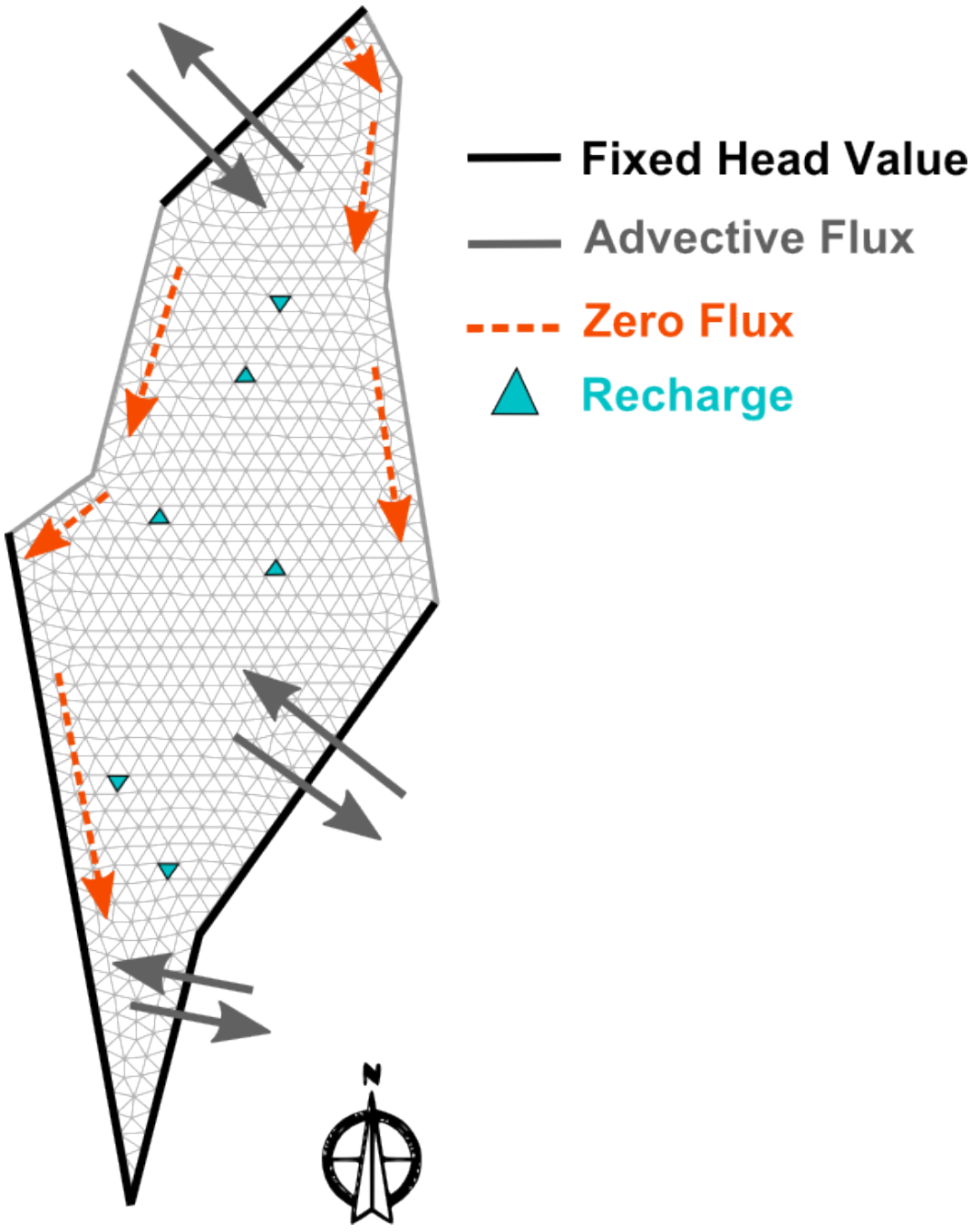

Figure 2.4: Boundary Conditions used for the finite element model. Dirichlet boundary condition in the northwest and southeast for groundwater flow equation, and Neumann boundary conditions in the northwest and southeast for the advection dispersion equation. Zero flux boundaries along the sides of the model domain

Table II.1 Model Parameters and Boundary conditions.

Parameter	Units	Value	Source
Medium T (medium sands)	km^2yr^{-1}	2.5e-3	Fetter (2001)
Low T (fine sands)	km^2yr^{-1}	2.5e-5	Fetter (2001)
Annual Recharge	myr^{-1}	50	Shamsuddah (2011)
Dispersivity	$kmyr^{-1}$	0.5-1.0	Gelhar (1992)
Diffusion Coefficient	$kmyr^{-1}$	1e-6	Flury (2002)
Initial salinity	g/l	6.3	Auerbach (2013)
Time zero	yrs	6000	Carbon Isotopes

Chapter III

RESULTS

3.1 Isotopes

The DIC in the groundwater ranges from ∼50-70 percent modern (PM) ^{14}C excluding the managed artificial recharge site (Table III.1,Figures 3.1,3.2). The MAR site, with forced surface water recharge, contains modern water and is not considered in the analysis of groundwater samples. The lowest PM DIC is found in the GW-11 site located in the northernmost extent of the groundwater sampling sites. The highest PM DIC is found in the GW-29 site, which is located in the southern half of the Polder. The GW-12 and GW-37 sites contains DIC that is 60-70 PM (Figure 3.2). The OxCal calibration software reports age ranges within the 95.4% probability interval; the average of the upper and lower age bounds is used in Table 1. Accounting for the PM DIC in recharge water from eq. 2, and using the most recent calibration curve, (*Reimer et al.*, 2013) the groundwater age ranges from ∼ 1500-5000 BP. Tritium was relatively high in the MAR site, and was detected in all of the sites.

3.2 Electromagnetic Induction

The electrical conductivity of the shallow subsurface generally increases towards the south of the Polder (Figure 3.3). The highest frequency (63030 Hz) induced a quadrature current,

Table III.1 Isotope results from 5 tubewells on Polder 32.[a]

Sample	PM ^{14}C	C1	OxCal C1	C2	OxCal C2	δ^{13}C (%)	TU
GW-11	51.1 ± 0.2	5550	6230	4440	4960	2.7	0.11 ± 0.02
GW-12	60.1 ± 0.2	4210	4660	3060	3280	3.8	0.05 ± 0.02
GW-29	75.6 ± 0.3	2310	2260	1160	1090	-8.6	0.02 ± 0.04
GW-37	70.7 ± 0.2	2870	2890	1720	1630	-5.7	0.08 ± 0.02
GW-MAR	104.2 ± 0.3	Modern	x	x	x	-19.3	3.42 ± 0.11

[a]All of the dates presented are YPB. MAR- Managed Artificial Recharge site, PM- percent modern C-14, C1- uncorrected ages from eq.1, OxCal C1- calibrated C1 ages, C2- corrected ages from eq. 2, OxCal C2- calibrated C2 ages, δ^{13}C- percent carbon-13, TU- tritium units.

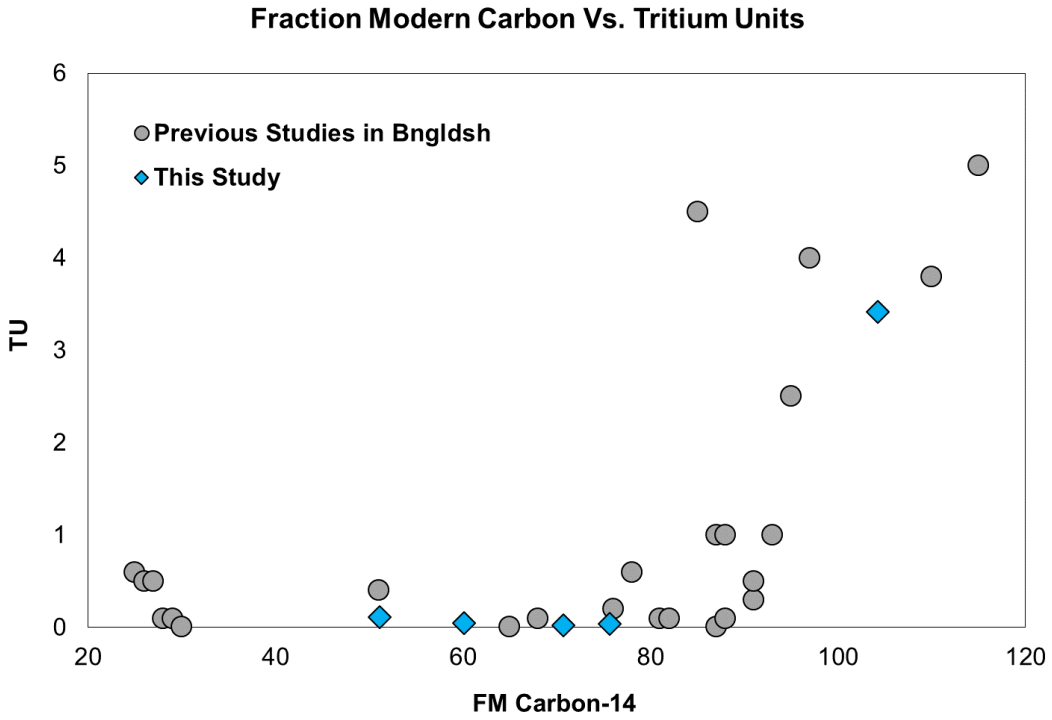

Figure 3.1: Scatter plot of tritium and carbon 14. Note the increase in TU around 87 percent modern carbon and the initial activity of carbon in equation 2.2. Previous studies from *Hoque and Burgess* (2012)

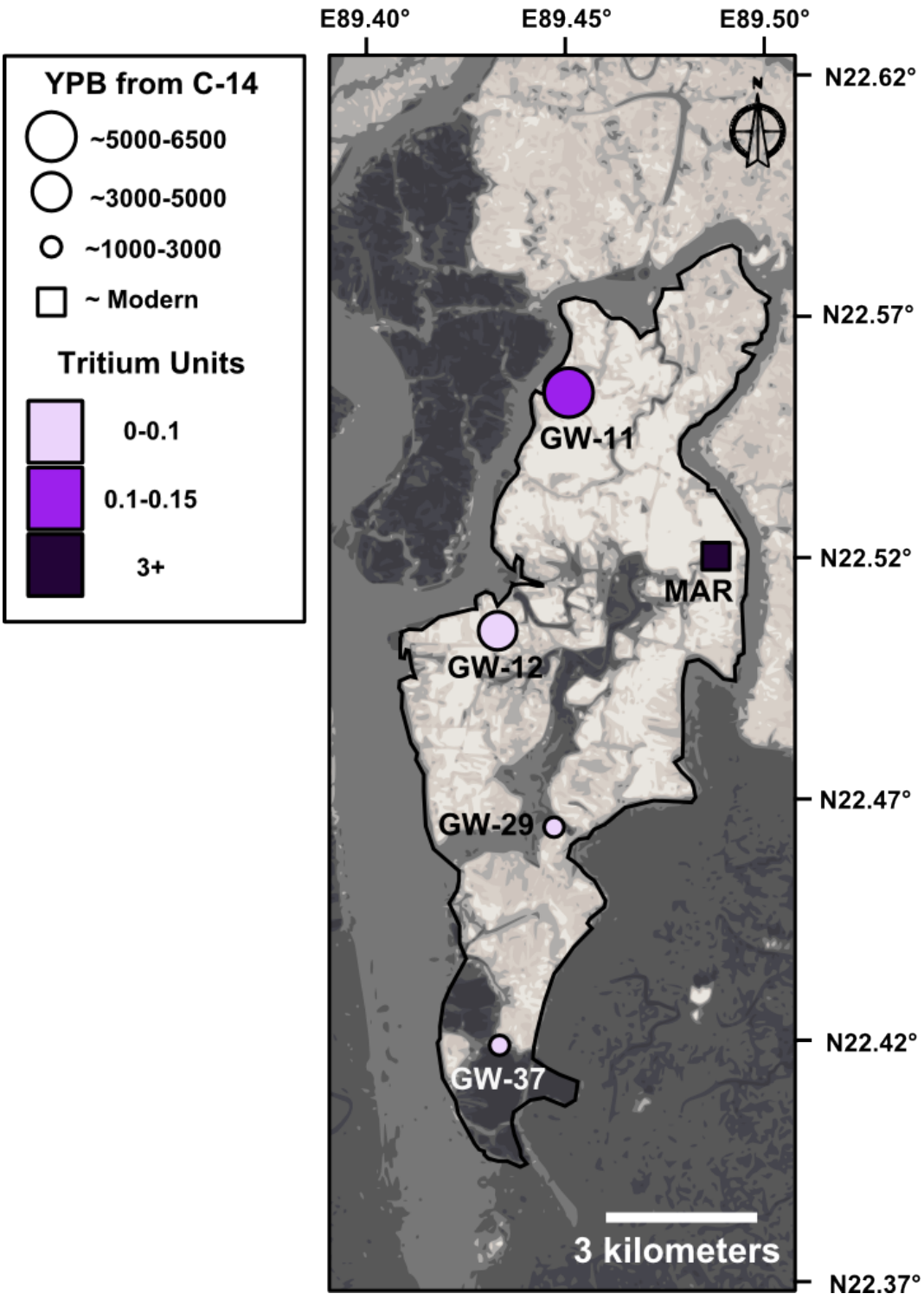

Figure 3.2: Results from isotope analysis. The carbon isotopes suggest older water in the north and younger water towards the south. Detectable tritium values were found in all of the wells, with a higher concentration in the north and the highest concentration at the MAR site.

that when converted to electrical conductivity (EC), records the highest EC on average, the lowest frequency (1530) records the lowest EC on average and the mid-range frequency (5310 Hz) records intermediate EC on average (Figure 3.3). The transects at a given frequency show lateral variation in conductivity. The vertical structure of the subsurface is estimated by the inversions of the EM signals for each frequency. The inversions reveal a more conductive geologic unit over a less conductive geologic unit for each transect, with lateral variability in thickness and sediment composition (Figure 3.3). EC is inversely related to hydraulic conductivity (*Smith and Sjogren*, 2006), so we interpret the high EC areas to represent areas of lower hydraulic conductivity (mud), and areas of low EC to be larger grain sediments with a higher hydraulic conductivity (sands).

3.3 Finite Element model

The model was run using two different transmissivity (T) scenarios, isotropic T (Fig. 3.4 A) and randomly generated anisotropic T (Fig. 3.4 B). The cyan elements are arbitrarily selected locations of direct recharge. The results to the flow equation (eq. 4) for the two different T scenarios are represented by A1 and B1 in Figure 3.4. The results to the solute transport equation (eq. 3) are represented by A2:A4 and B2:B4. Different T scenarios change the direction and magnitude of the flow vectors. Scenario A generally advects water away from the recharge sites towards the lower head boundaries. The salinity transport for scenario A shows a gradual freshening progression with fresher elements located around recharge locations. Scenario B generated vectors in complex patterns reflecting the random

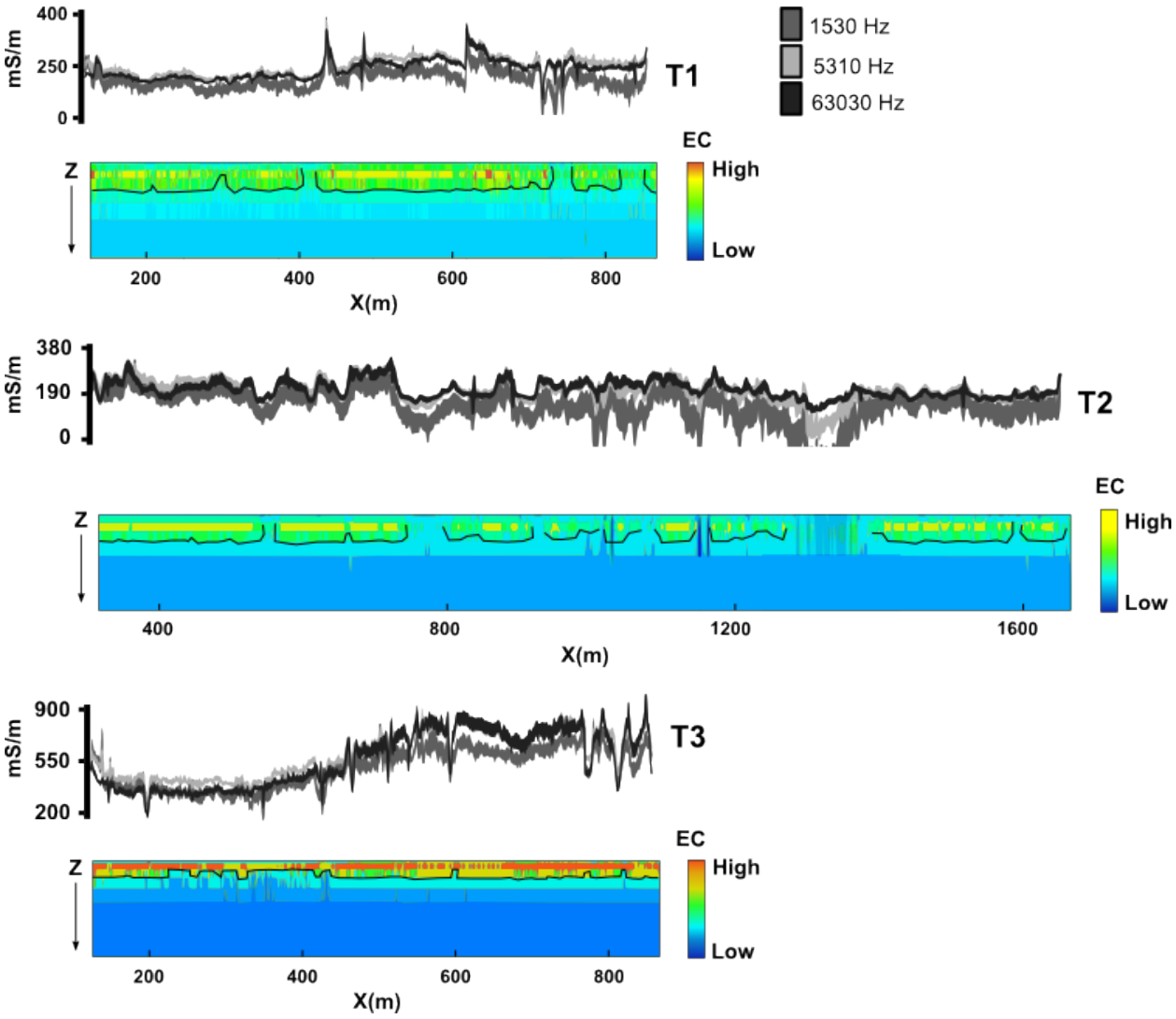

Figure 3.3: The electrical conductivity (EC) results for three different frequencies, for three transects. An inversion model was built for each transect using the inphase and quadrature data. The inversions reveal a higher EC unit (delineated with a black line), underlain by units with a lower EC, which is interpreted as muds underlain by sands. A depth was not assigned for the inversion, as each layered earth model should be viewed in light of relative variability in thickness and sediment composition.

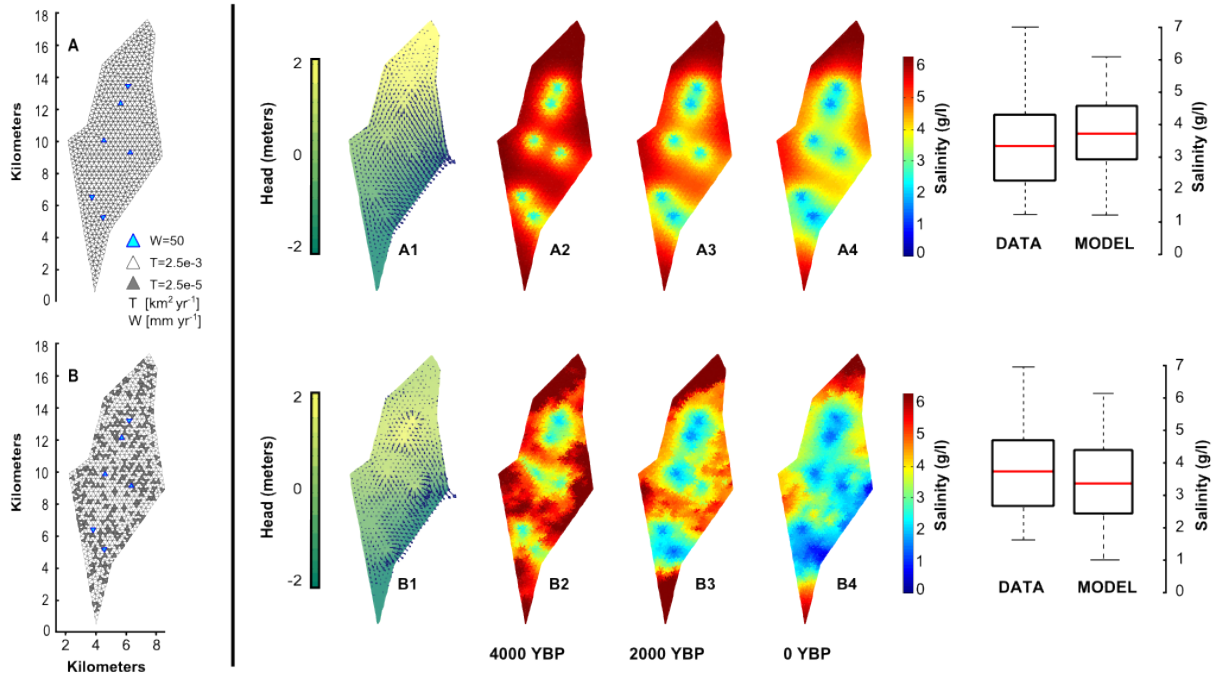

Figure 3.4: Results from the FEM model. The left side of the figure is the two different stratigraphy scenarios (A) isotropic transmissivity and (B) randomly generated anisotropic transmissivity. A1 and B1 are the solutions to the flow equation (eq. 4) for each scenario. The solute transport equation was calculated for 6000 yrs using a starting salinity value of 6.3 g/l. A4 and B4 are the present day concentrations calculated by the model. The box and whisker plots show the salinity concentrations currently on Polder 32 (data) and the modelled concentrations for each scenario (A4 and B4)

assignment of transmissivities. The salinity transport for scenario B provides similar patterns to A, but exhibits greater spatial variance than scenario A (Figure 3.4). The box and whisker plots show that both scenarios generated salinities similar to the current day salinity values.

Chapter IV

DISCUSSION

The carbon isotopes indicate connate groundwater that was deposited between 1000-6500 years BP, and the tritium present in all the samples suggests the possible infiltration of small amounts fresh meteoric recharge. The groundwater age range reflects the delta building processes occurring at the time of aquifer deposition. As sea-level rise slowed around 7000 years BP, the GBM delta changed from an aggradational system to a progradational system (*Goodbred and Kuehl*, 2000). Muddy sands were deposited on the lower delta creating the shallow aquifer. The confining unit was subsequently deposited during annual tidal channel flooding prior to polder construction. The chemistry of the connate water is a mixture of the tidal channel water composition during aquifer deposition, which was most likely between 5-10 g/l salinity (*Auerbach*, 2013). The ages and current salinities of the groundwater support a conceptual mixing model that does not involve interaction with modern seawater from the Bay of Bengal.

The EM results suggest that the confining mud unit varies in thickness across the polder, which is consistent with sediment data (Figure 2.2). The inversion indicates that there are areas where the mud cap is thin or non-existent, which would allow vertical infiltration of rain water during the wet season. Previous studies have used frequency domain EM to delineate areas of direct recharge based on soil texture (*Cook et al.*, 1989, 1992; *Aziz et al.*,

2008). There is concern that fixed-geometry broadband EM instruments, such as the GEM-2, prevent the construction of meaningful layered earth models (*McNeill*, 1996). This is due to equivalence, where many different layered earth models will give the same measured response with frequency. Other investigations suggest this problem can be overcome with a source cancellation scheme embedded in the receiver coil, which is present in the GEM-2 (*Won*, 2003). Regardless of the debate surrounding the use of broadband EM induction to resolve layered earth models, this current investigation reveals much lateral variability in EC for each transect (Figure 3.3). The inversions do not use discrete depth values, due to some of the issues mentioned above. The vertical profile should be interpreted in light of the internal variation within each model, and can not be accurately compared between different transects as each model has a different mean EC, which is related to the bulk grain size (*Triantafilis and Lesch*, 2005). There exists significantly varied EM responses across the polder that suggest changes in sediment texture – allowing greater recharge in isolated locations. Without significant head gradients to drive flow, the freshwater entering the aquifer will slowly advect and propagate throughout the aquifer by mechanical dispersion and molecular diffusion (Figure 4.2). The embankments protecting the polder prevent frequent tidal channel inundation and the addition of saltwater to the aquifer, suggesting that recharge water is primarily fresh, meteoric water (*Auerbach*, 2013). Complex delta forming processes have most likely created preferential flow paths for groundwater through coarse sands of paleochannels (*Mulligan et al.*, 2007). It is unclear whether these channels are connected beneath the entire polder, and would require a large scale geophysical effort to determine

whether they are continuous.

The isotope data and GEM results were used to parametrize the FEM. The carbon isotopes provided an initial time for the model of 6,000 years. This value was chosen as it roughly represents the maximum possible age of the shallow groundwater (Table III.1). The tritium concentrations and GEM results support the possibility of direct recharge, at least through discrete sites of lower mud content. Based on literature, we allowed 50 mm of rainwater to infiltrate into the aquifer annually through six arbitrarily chosen recharge sites (*Shamsudduha et al.*, 2011). The numerical model confirms what the other data suggests: the salinity distribution can be theoretically explained by a slow freshening of connate tidal channel water by direct meteoric recharge. The FEM also demonstrates that the system is advection dominated, and is insensitive to minor changes in aquifer architecture (Figure 3.4). Heterogeneous transmissivity allows the water to advect with slightly higher velocities as the areas of preferential flow serve as conduit-like features, but the overall salinity composition does not change significantly.

The proposed conceptual model consists of a simplified regional hydrogeological system composed of three distinct aquifers that are likely hydrologically connected (*Zahid et al.*, 2008; *Kinniburgh and Smedley*, 2001). In reality, the lithology of these aquifers is complex and the specific heterogeneity is not well defined (figure 4.2). The salinity in the deeper aquifers is thought to originate from seawater intrusion (*Rahman et al.*, 2000), paleoseawater, or some combination of rock dissolution and ion exchange (*Rahman et al.*, 2011a). We propose that the shallow aquifer salinity can be most easily explained in light of the land

building processes during the last 10,000 years. The carbon isotopes suggest connate water, the tritium isotopes and GEM transects indicate small amounts of recharge and the FEM model elucidates the transport processes that slowly advect infiltrating recharge throughout the shallow aquifer. The freshwater lenses supplied by direct recharge are susceptible to salinity degradation from over-pumping (*Essaid*, 1986; *Panday et al.*, 1993; *Motz*, 1995). These finite volumes of fresh drinking water are poorly delineated and sustainable pumping rates are entirely unknown. Without detailed information on the location, fresh water recharge rates, and extent of the freshwater lenses, there is risk of overpumping these local sources and contaminating with laterally advected saline groundwater.

The origin of the shallow brackish groundwater in low lying coastal areas involves a complicated story of concurrent landscape and hydrological evolution throughout the Holocene (*Delsman et al.*, 2013; *Tran*, 2012; *Bahar and Reza*, 2010; *Wang et al.*, 2013; *Goodbred and Kuehl*, 2000). Varying sediment supply rates, tectonic activity, river avulsions, basin subsidence, eustatic sea-level change and anthropogenic alterations have all influenced aquifer construction and groundwater chemistry. *Delsman et al.* (2013) notes that coastal groundwater reserves are rarely in equilibrium with current boundary conditions, which greatly complicates modeling the distribution of water salinities. The current groundwater condition of coastal aquifer systems must by explored in light of the historical development of groundwater salinity in combination with present day hydrological processes.

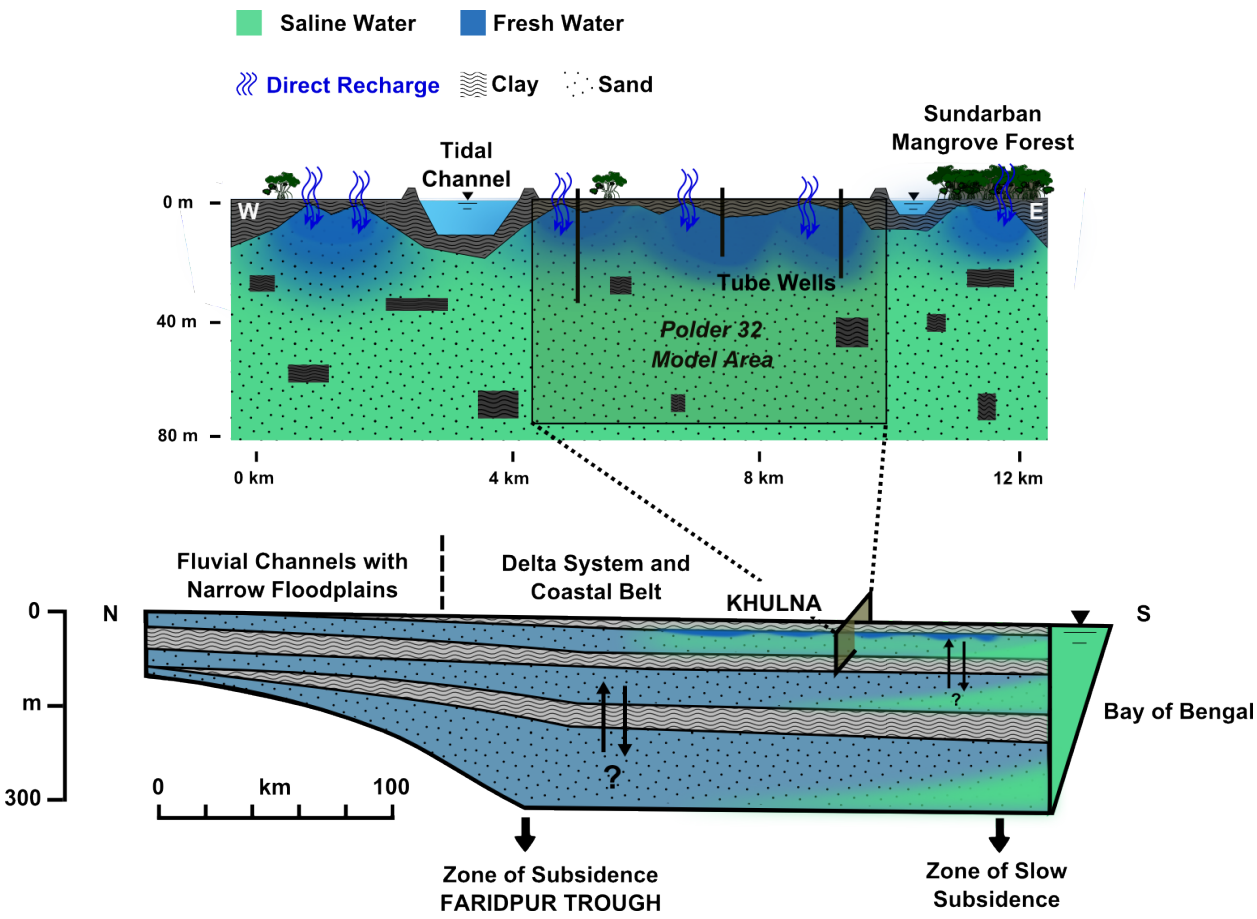

Figure 4.1: Conceptual model of salinity distribution in the regional aquifers and in the shallow aquifer beneath the Polder. The regional characterization schematic is a simplified representation of the aquifer systems presented in *Kinniburgh and Smedley* (2001). We propose a simple mixing model of connate brackish groundwater with freshwater lenses sustained by annual meteoric recharge.

Appendix A

GEM RESULTS

This appendix includes the electrical conductivity data from each transect (Fig. A.1), and a explanation of the parameters used in the inversion program. The University of British Columbia Geophysical Inversion Facility (UBC-GIF) produces the inversion program, EM1DFM (*Farquharson*, 2000) The inversion program is designed to construct 1D models using geophysical frequency domain data. EM1DFM requires a set of input files, and the contents are listed below with brief explanations of what each parameter provides to the model construction. For more information, the reader is referenced to the supporting material of the UBC-GIF websites.

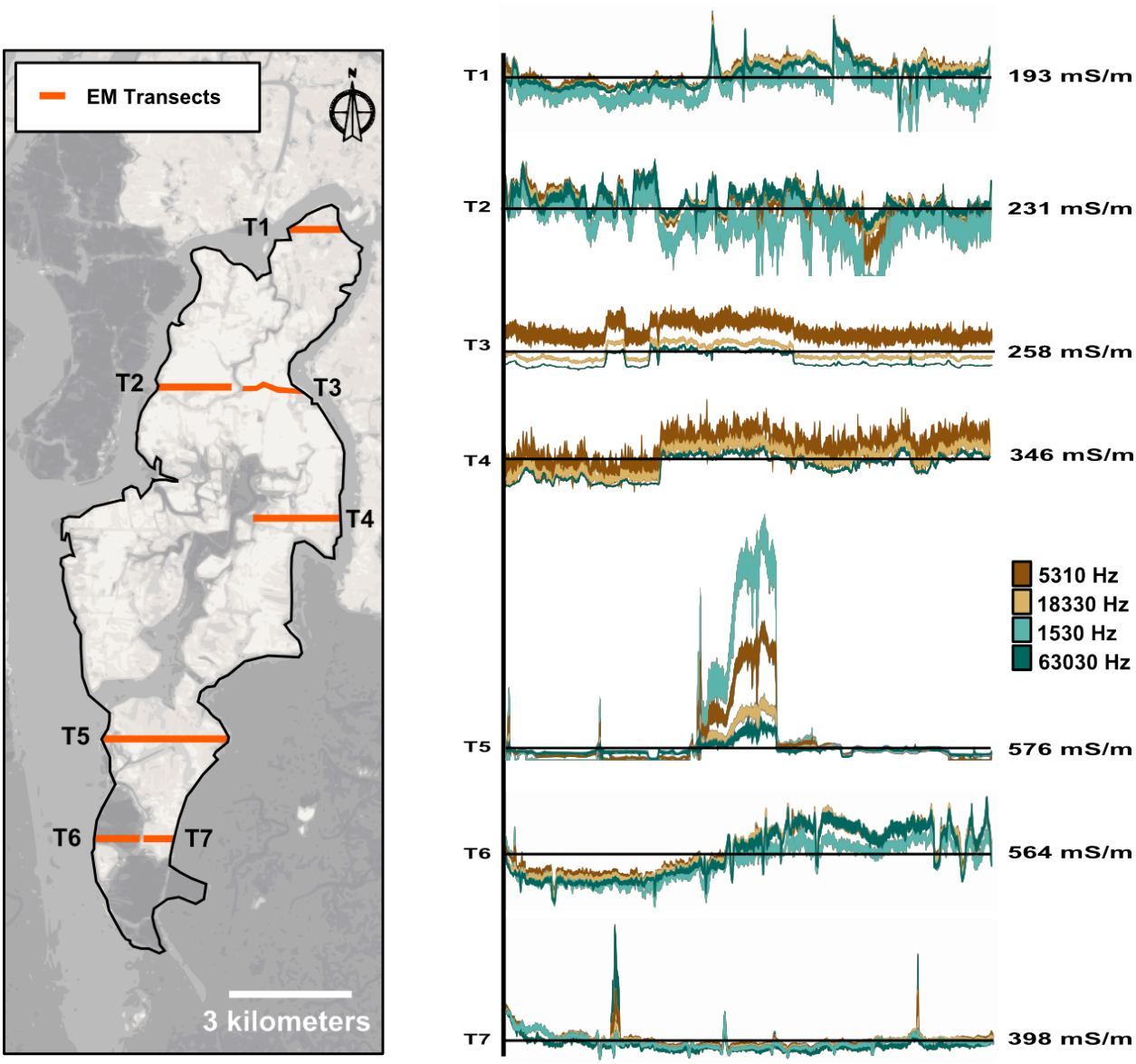

Figure A.1: Complete results from GEM transects. The colors are for the different frequencies and the black line and the value to the right of each transect is the mean conductivity of all of the frequencies. The lowest frequency, 450 Hz, is not shown in figure A.1 because of the noise associated with the data. Transect T3 was taken along the length of an embankment, hence the curve in the transect and the uniqueness of the electrical conductivity results. Note the high conductivity values of T5. We attribute these values to locations of high saline water, and do not interpret the results to provide information for grain size, as the conductivities are much higher than the other transects.

A.1 lodi.in

The lodi file is used to format the raw frequency data into the required format.

```
Inputfilename.xyz                          !Input file name
Outputfilename.obs                         !Output file name
12                                         !number of columns
ignore                                     !ignore the first column
x                                          !x coordinate data
y                                          !y coordinate data
z m                                        !Elevation of GEM in meters
1530. z 3. z m 1.6 0. 1 i 5. 0.1           !Fifth column
1530. z 3. z m 1.6 0. 1 q 5. 0.1           !Sixth column
5310. z 3. z m 1.6 0. 1 i 5. 0.1           !Seventh column
5310. z 3. z m 1.6 0. 1 q 5. 0.1           !Eighth column
18330. z 3. z m 1.6 0. 1 i 5. 0.1          !Ninth column
18330. z 3. z m 1.6 0. 1 q 5. 0.1          !Tenth column
63030. z 3. z m 1.6 0. 1 i 5. 0.1          !Eleventh column
63030. z 3. z m 1.6 0. 1 q 5. 0.1          !Twelfth column
al                                         !Use each sounding
```

A.2 start.con

The start file is the starting conductivity model for the soundings. The first number is the number of layers, and the following numbers are, on the left, the thickness (m) of the layer and on the right, the starting conductivity of each later (S/m).

```
8
3   0.5
3   0.5
3   0.5
3   0.05
3   0.05
3   0.05
3   0.05
0   0.05
```

A.3 em1dfm.in

The em1dfm file is the main input file for the program, and contains the parameters used in constructing the model. It allows the user to choose the model type, additional weights, inversion algorithm and other options.

```
input          ! Root for output file names
output.obs     ! Name of the observations file
1              ! model type
start.con      ! Starting conductivity model file
start.con      ! Reference (smallest) conductivity model file
0.             ! Reference susceptibility model file
NONE           ! Reference (flattest) conductivity model file
NONE           ! Additional weights
0.01 1.        ! alpha_s & alpha_z
3              ! Type of inversion algorithm
0.5            ! Max. decrease of trad
15             ! Max number of iterations in the inversion
DEFAULT        ! Small number for convergence tests
DEFAULT        ! Number of explicit evaluations of Hankel kernels
1              ! Flag for amount of output
```

Appendix B

FINITE ELEMENT METHOD

The numerical methods implemented in the code from Appendix A closely followed the finite element method presented in chapters 10 and 11 of the AGU ebook, Numerical Methods in the Hydrological Sciences (*Hornberger and Wiberg*, 2005). The differential equations (eq. 2.3 and 2.4) were solved over a mesh using the Galerkin weighted residual method. Some of the important conceptual and mathematical aspects are outlined below.

B.1 Background

Due to the complex geometry of the proposed problem–modelling salinity changes through time over an irregularly shaped mesh with variable transmissivity–the finite element method is more desirable than the finite difference method. The basis of the finite element method is to determine a functional approximation to the differential equations. This gives the advantage of obtaining a continuous function over the mesh rather than discrete approximations at specific nodes. The finite element method also provides simple boundary conditions, and the freedom to change easily the input parameters for specific elements.

B.2 Steady State Groundwater Flow Equation

The ground water flow equation in two dimensions:

$$\frac{\partial}{\partial x}\left(T\frac{\partial h}{\partial x}\right)+\frac{\partial}{\partial y}\left(T\frac{\partial h}{\partial y}\right)+R=0, \tag{B.1}$$

The general coordinates for an element are,

$$\varepsilon_n(x,y)=\frac{1}{2\Delta}(\alpha_n+\beta_n x+\gamma_n y), \tag{B.2}$$

Where,

$$\begin{aligned}\alpha_i &= x_j z_k - x_k z_j\\ \beta_i &= y_j - y_k\\ \gamma_i &= x_k - x_j.\end{aligned} \tag{B.3}$$

The approximation of the head for each element, is the sum of the basis functions multiplied by the head at each node,

$$\hat{h}=\varepsilon_i h_i+\varepsilon_j h_j+\varepsilon_k h_k \tag{B.4}$$

And the change in head in the x direction is,

$$\frac{\partial h}{\partial x}=\frac{1}{2\Delta}T_x\left[\beta_i h_i+\beta_j h_j+\beta_k h_k\right] \tag{B.5}$$

and using the notation introduced in eq. B.3, the global conductance matrix can be written as follows,

$$T_x \begin{bmatrix} \frac{\beta_i\beta_i}{4\Delta} & \frac{\beta_i\beta_j}{4\Delta} & \frac{\beta_i\beta_k}{4\Delta} \\ \frac{\beta_j\beta_i}{4\Delta} & \frac{\beta_j\beta_j}{4\Delta} & \frac{\beta_j\beta_k}{4\Delta} \\ \frac{\beta_k\beta_i}{4\Delta} & \frac{\beta_k\beta_j}{4\Delta} & \frac{\beta_k\beta_k}{4\Delta} \end{bmatrix} + T_y \begin{bmatrix} \frac{\gamma_i\gamma_i}{4\Delta} & \frac{\gamma_i\gamma_j}{4\Delta} & \frac{\gamma_i\gamma_k}{4\Delta} \\ \frac{\gamma_j\gamma_i}{4\Delta} & \frac{\gamma_j\gamma_j}{4\Delta} & \frac{\gamma_j\gamma_k}{4\Delta} \\ \frac{\gamma_k\gamma_i}{4\Delta} & \frac{\gamma_k\gamma_j}{4\Delta} & \frac{\gamma_k\gamma_k}{4\Delta} \end{bmatrix}$$

B.3 Advection Dispersion Equation

$$\frac{\partial c}{\partial t} = -u_x \frac{\partial c}{\partial x} - u_y \frac{\partial c}{\partial y} + D_x \frac{\partial^2 c}{\partial x^2} + D_y \frac{\partial^2 c}{\partial y^2} + \gamma, \tag{B.6}$$

global "conductance" matrix for the advection terms can be written as follows,

$$u_x \begin{bmatrix} \frac{\beta_i\beta_i}{6} & \frac{\beta_i\beta_j}{6} & \frac{\beta_i\beta_k}{6} \\ \frac{\beta_j\beta_i}{6} & \frac{\beta_j\beta_j}{6} & \frac{\beta_j\beta_k}{6} \\ \frac{\beta_k\beta_i}{6} & \frac{\beta_k\beta_j}{6} & \frac{\beta_k\beta_k}{6} \end{bmatrix} + u_y \begin{bmatrix} \frac{\gamma_i\gamma_i}{6} & \frac{\gamma_i\gamma_j}{6} & \frac{\gamma_i\gamma_k}{6} \\ \frac{\gamma_j\gamma_i}{6} & \frac{\gamma_j\gamma_j}{6} & \frac{\gamma_j\gamma_k}{6} \\ \frac{\gamma_k\gamma_i}{6} & \frac{\gamma_k\gamma_j}{6} & \frac{\gamma_k\gamma_k}{6} \end{bmatrix}$$

and for the dispersion terms,

$$D_x \begin{bmatrix} \frac{\beta_i\beta_i}{4\Delta} & \frac{\beta_i\beta_j}{4\Delta} & \frac{\beta_i\beta_k}{4\Delta} \\ \frac{\beta_j\beta_i}{4\Delta} & \frac{\beta_j\beta_j}{4\Delta} & \frac{\beta_j\beta_k}{4\Delta} \\ \frac{\beta_k\beta_i}{4\Delta} & \frac{\beta_k\beta_j}{4\Delta} & \frac{\beta_k\beta_k}{4\Delta} \end{bmatrix} + D_y \begin{bmatrix} \frac{\gamma_i\gamma_i}{4\Delta} & \frac{\gamma_i\gamma_j}{4\Delta} & \frac{\gamma_i\gamma_k}{4\Delta} \\ \frac{\gamma_j\gamma_i}{4\Delta} & \frac{\gamma_j\gamma_j}{4\Delta} & \frac{\gamma_j\gamma_k}{4\Delta} \\ \frac{\gamma_k\gamma_i}{4\Delta} & \frac{\gamma_k\gamma_j}{4\Delta} & \frac{\gamma_k\gamma_k}{4\Delta} \end{bmatrix}$$

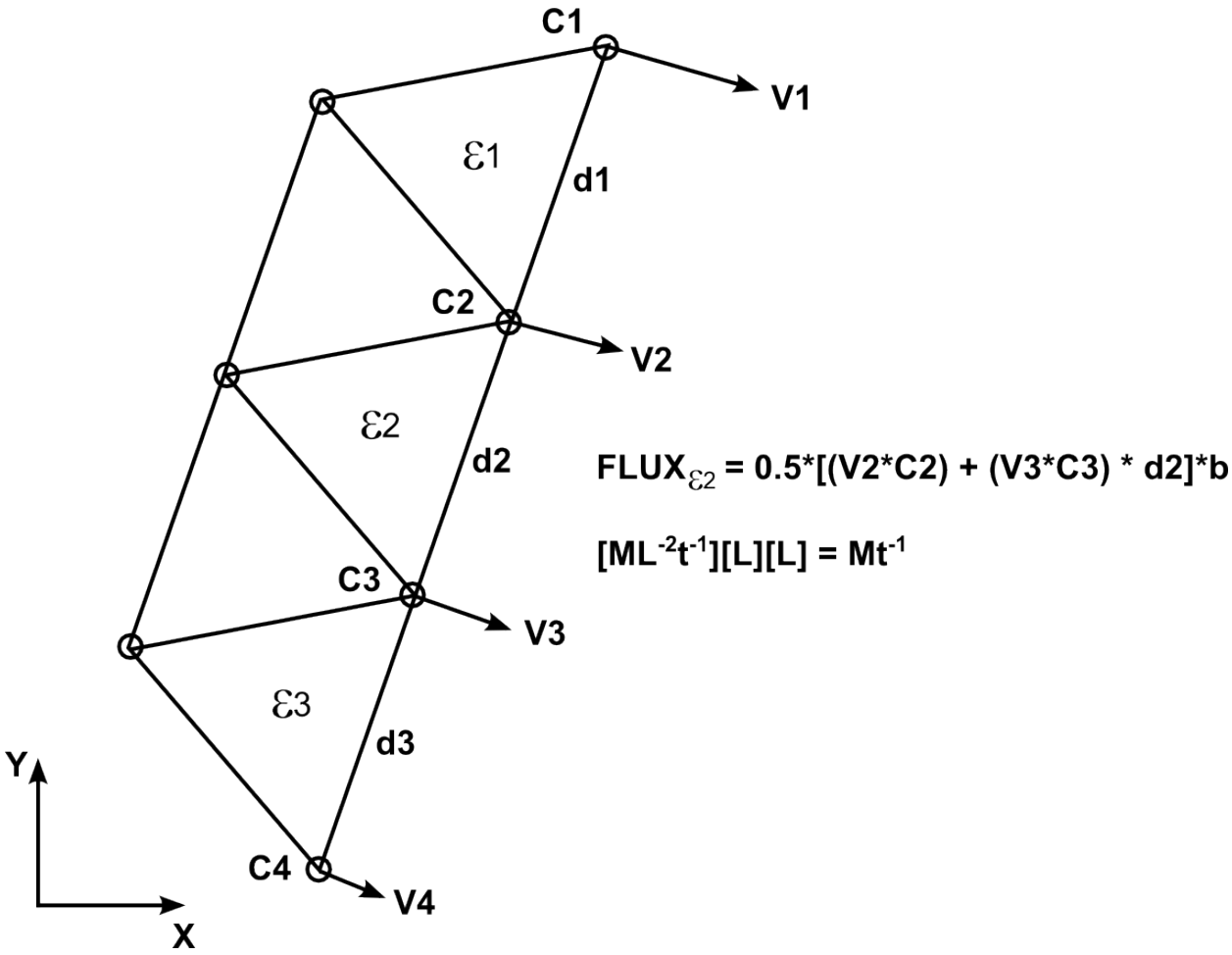

Figure B.1: An example calculation for a Neumann boundary condition. The concentration at the boundary nodes and the velocity components normal to the boundary are used to calculate the mass flux out of the model domain each time step.

B.4 Flux Boundary Conditions

The flux boundary conditions were handled in a straightforward manner. The concentrations and normal velocity components at the two end nodes of a boundary line segment were integrated over the segment and multiplied at each time step yielding a mass flux out of the element.

Appendix C

MATLAB CODE

```
%MATLAB code to solve the steady state groundwater flow equation and the
%advection dispersion equation using the finite element method. The work
%was done as part of a masters project at Vanderbilt University from
%2012-2014.

%Authors: Scott Worland, George Hornberger
%Corresponding Author: Scworland@usgs.gov
%This code uses: distmesh2d.m v1.1, 2012 Per-Olof Persson

%The script requires:

%(1)distmesh2d (and associated functions): persson.berkeley.edu/distmesh
%(2)trigradient: mathworks.com/matlabcentral/fileexchange/36837
%(3)triquiver: mathworks.com/matlabcentral/fileexchange/38856

% VARIABLES/VECTORS/MATRICES
%       T:              Transmissivity of aquifer (km^2/yr)
%       T2:             Lower transmissivity value
%       w:              Recharge rate (mm/yr)
%       n:              Porosity
%       alpha:          Dispersivity (km) (Gelhar,1992)
%       De:             Molecular diffusion (km^2/yr)(Flury, 2002)
%       c0:             Starting salnity concentration (g/l)
%       tend:           Total time (yrs)
%       dt:             Time step (yrs)
%       cr:             Concentration of the recharge water(g/l)
%       b:              Depth of aquifer (km)
%       pv:             vertex points
%       p:              Node coordinates (nx2)
%       t:              Triangle indices (nx2)
%       elemx:          X coordinates for each element (nx3)
%       elemy:          Y coordinates for each element (nx3)
%       bound:          Bounding node number (nx2)
%       Bn#:            Index of each boundary segment in bound (nx1)
%       Bp#:            Index of each boundary segment in p (nx1)
%       nodex:          coordinates for xnodes (nx1)
%       nodey:          coordinates for ynodes (nx1)
%       E#:             Index of boundary elements
%       topelem:        Index of elements along top boundary
%       bottomelem1:    Index of elements along bottom right boundaries
%       topnodes:       Index of nodes along top boundary
```

```
%       bnodes1:        Index of nodes along bottom right boundaries
%       randT:          Randomly selected elements to assign low T
%       relem:          Recharge elements
%       nnodes:         Number of nodes
%       nelem:          Number of elements
%       G:              Element conductance matrix (sparse nxn)
%       delta:          area of element
%       rhs:            Right hand side vector for flow equation
%       h:              Solution to gw flow equations (h=heads)
%       n:              Porosity
%       hx:             head gradient x direction with node as vertex
%       hy:             head gradient y direction with node as vertex
%       u:              velocity gradient x direction on face
%       v:              velocity gradient y direction on face
%       Dx:             Lateral hydrodynamic dispersion coefficient
%       Dy:             Longitudinal hydrodynamic dispersion coefficient
%       S:              Global salinity "conductance" matrix (sparse nxn)
%       P:              Time matrix (sparse nxn)
%       F:              Global salinity "conductance" matrix + time matrix
%       rhs2:           Right hand side vector for ADE
%       BV:             Velocity component normal to bottom boundary
%       TV:             Velocity component normal to top boundary
%       EV:             element volume

clear all

T = 2.5e-3; % km^2/yr (k for med sands=9e-7 m/s, b=75 meters)
T2 = T;
w = 50; %mm/yr for each "recharge site"- annual rainfall is 2000 mm/year
w = w*1e-6; %recharge rate (km/yr)
n = 0.4; %Porosity
alpha = 0.5; % 0.1-1 km (Gelhar,1992)
De = 3e-6; % 3e-6 km^2/yr (Flury, 2002)
c0 = 6.3; %g/l
tend = 2000; %years
dt = 1; %years
cr = 0; %Recharge concentration
b = 0.075; %Depth of aquifer in km (~75 meters)


%Below is the code to generate the mesh. For more information, read
%distmesh2d, as it is well documented internally

BBox=[0,0; 10,20]; %bounding box in which mesh will be plotted
Edge=0.3; %starting edge length for model (smaller number=more elements)
pv=[4 1; 2.2 11; 3.5 12; 4.5 16; 7.5 19; 8 18; 7.75 15; 8.5 10; 5 5; 4 1];
[p,t]=distmesh2d(@dpoly,@huniform,Edge,BBox,pv,pv);
set(gcf, 'color', 'w');
figure(1);
title('Finite Element Mesh of Polder 32');
hold on
```

```
%Creates matrices of x and y values for each node of an element
elemx=[p(t(:,1)) p(t(:,2)) p(t(:,3))];
elemy=[p(t(:,1),2) p(t(:,2),2) p(t(:,3),2)];

%Below find the boundary edges of interest. Should work for a range of
%element sizes (Edge values above), but may become buggy if the shape of
%the mesh is changed
e = boundedges(p,t); be = unique(e);  %finds bounding edges
nodes=t; nodex=p(:,1); nodey=p(:,2); %x and y node vectors
bound=p(be(:),1:2); %Creates vector of bounding node coordinates

%bound is node coordinates for all bounding nodes.
d=max(max(pv))/Edge;

%loops through vertices to find index of vertices (pvi) in bound
for i=1:length(pv)-1;
pvi(i)=find(pv(i,1)==bound(:,1) & pv(i,2)==bound(:,2));
end
pvi=pvi';

%Creates a x and y matrix with lines between vertices in pv
for i=1:length(pv)-1;
p2=polyfit([pv(i);pv(i+1)],[pv(i,2);pv(i+1,2)],1);
x(:,i)=linspace(pv(i),pv(i+1),100)';
y(:,i)=polyval(p2,x(:,i));
end

%Rounds all vectors to tenth
x2=round(x/0.1)*0.1;
y2=round(y/0.1)*0.1;
bx=round(bound(:,1)/0.1)*0.1;
by=round(bound(:,2)/0.1)*0.1;

%finds index of each boundary segment in bound... bound(Bn1,Bn2...)
for i=1:length(pv)-1;
eval(['Bn' num2str(i) ' = find(ismember(bx,x2(:,i)) & ismember(by,y2(:,i)));']);
end

%finds index of each boundary segment in p... p(Bp1,Bp2...)
j={Bn1,Bn2,Bn3,Bn4,Bn5,Bn6,Bn7,Bn8,Bn9};
for i=1:length(pv)-1;
eval(['Bp' num2str(i) ' = find(ismember(p(:,1), bound(j{1,i})));']);
end

%Linear indexing for bounding elements
for i=1:length(pv)-1;
eval(['E' num2str(i)...
    ' = find(ismember(elemx, bound(j{1,i},1)) & ismember(elemy, bound(j{1,i},2)));']);
end
```

```
elemx=elemx;
elemy=elemy;
%Subcript indexing for bounding elements
[E1,j1]= find(ismember(elemx,bound(Bn1)) & ismember(elemy,bound(Bn1,2)));
[E2,j2]= find(ismember(elemx,bound(Bn2)) & ismember(elemy,bound(Bn2,2)));
[E3,j3]= find(ismember(elemx,bound(Bn3)) & ismember(elemy,bound(Bn3,2)));
[E4,j4]= find(ismember(elemx,bound(Bn4)) & ismember(elemy,bound(Bn4,2)));
[E5,j5]= find(ismember(elemx,bound(Bn5)) & ismember(elemy,bound(Bn5,2)));
[E6,j6]= find(ismember(elemx,bound(Bn6)) & ismember(elemy,bound(Bn6,2)));
[E7,j7]= find(ismember(elemx,bound(Bn7)) & ismember(elemy,bound(Bn7,2)));
[E8,j8]= find(ismember(elemx,bound(Bn8)) & ismember(elemy,bound(Bn8,2)));
[E9,j9]= find(ismember(elemx,bound(Bn9)) & ismember(elemy,bound(Bn9,2)));

jj={E1,E2,E3,E4,E5,E6,E7,E8,E9};
for i=1:length(pv)-1;
eval(['E' num2str(i),' = unique(jj{1,i});']);
end

topelem=E4;
bottomelem1=[E8;E9];
topnodes = Bp4;
bnodes1=unique([Bp9;Bp8]);

%Below is where the elements are chosen to assign a random transmissivity
%and the elements are selected for the injection wells

%selects random elements for lower transmissivity
randT=randperm(length(nodes),300);
%Uncomment the below code to see which elements were selected
%  for i=1:length(randT);
%  patch(elemx(randT(i),:),elemy(randT(i),:),[0.3320 0.4180 0.1836]);
%      drawnow
%  end

%internal elements to assign recharge values to
relem=[156 939 759 586 680 898];

rech_elem=nodes(relem,:);
 for i=relem
 patch(nodex(nodes(i,:),:),nodey(nodes(i,:),:),[0 1 1]);
     drawnow
 end

%Below is the global flow matrices with potentially different
%transmissivities

nnodes=length(p); nelem=length(nodes);
G=sparse(nnodes,nnodes); % zero matrix in sparse format: zeros(G) would be "dense"
for elem=1:nelem  % integration over one triangular element
  i = nodes(elem,1); j = nodes(elem,2); k = nodes(elem,3);
  enodes=nodes(elem,:); % row of t = node numbers of the 3 corners of triangle e
```

```
  Pe=[ones(3,1),p(enodes,:)]; % 3 by 3 matrix with rows=[1 xcorner ycorner]
  delta=(abs(det(Pe))/2); % area of triangle (km^2) e = half of parallelogram area

  %betas and gammas are node coefficients
    betai = nodey(j) - nodey(k);
    betaj = nodey(k) - nodey(i);
    betak = nodey(i) - nodey(j);
    gammai = nodex(k) - nodex(j);
    gammaj = nodex(i) - nodex(k);
    gammak = nodex(j) - nodex(i);

    %Assigns transmissivity values based on randT
    x = ismember(i,nodes((randT),1));
    if x==0
    G(i,i) = G(i,i) + T*betai*betai/(4*delta) + T*gammai*gammai/(4*delta);
    G(i,j) = G(i,j) + T*betai*betaj/(4*delta) + T*gammai*gammaj/(4*delta);
    G(i,k) = G(i,k) + T*betai*betak/(4*delta) + T*gammai*gammak/(4*delta);
    G(j,i) = G(j,i) + T*betaj*betai/(4*delta) + T*gammaj*gammai/(4*delta);
    G(j,j) = G(j,j) + T*betaj*betaj/(4*delta) + T*gammaj*gammaj/(4*delta);
    G(j,k) = G(j,k) + T*betaj*betak/(4*delta) + T*gammaj*gammak/(4*delta);
    G(k,i) = G(k,i) + T*betak*betai/(4*delta) + T*gammak*gammai/(4*delta);
    G(k,j) = G(k,j) + T*betak*betaj/(4*delta) + T*gammak*gammaj/(4*delta);
    G(k,k) = G(k,k) + T*betak*betak/(4*delta) + T*gammak*gammak/(4*delta);
    else
    G(i,i) = G(i,i) + T2*betai*betai/(4*delta) + T2*gammai*gammai/(4*delta);
    G(i,j) = G(i,j) + T2*betai*betaj/(4*delta) + T2*gammai*gammaj/(4*delta);
    G(i,k) = G(i,k) + T2*betai*betak/(4*delta) + T2*gammai*gammak/(4*delta);
    G(j,i) = G(j,i) + T2*betaj*betai/(4*delta) + T2*gammaj*gammai/(4*delta);
    G(j,j) = G(j,j) + T2*betaj*betaj/(4*delta) + T2*gammaj*gammaj/(4*delta);
    G(j,k) = G(j,k) + T2*betaj*betak/(4*delta) + T2*gammaj*gammak/(4*delta);
    G(k,i) = G(k,i) + T2*betak*betai/(4*delta) + T2*gammak*gammai/(4*delta);
    G(k,j) = G(k,j) + T2*betak*betaj/(4*delta) + T2*gammak*gammaj/(4*delta);
    G(k,k) = G(k,k) + T2*betak*betak/(4*delta) + T2*gammak*gammak/(4*delta);
    end
end

%Set boundary conditions and solve flow equation
rhs = zeros(nnodes,1);
w_elem=rech_elem;
rr = w*delta; %volume/time
for i = 1:length(topnodes);
    rhs(topnodes(i)) = 1; %Elevation of top boundary(km)
    G(topnodes(i),:) = zeros(1,nnodes);
    G(topnodes(i),topnodes(i)) = 1;
end
for j = 1:length(bnodes1);
    rhs(bnodes1(j)) = 0.996; %Elevation of bottom boundary (km)
    G(bnodes1(j),:) = zeros(1,nnodes);
    G(bnodes1(j),bnodes1(j)) = 1;
end
for k=w_elem;
```

```
    rhs(k)= rhs(k) + rr/3; %Add in recharge to flow equation
end
h=G\rhs;

%Calculate flow vectors for nodes and the center of each element
[hx,hy]=trigradient(p(:,1),p(:,2),-h,nodes);
[u,v]=trigradient(p(:,1),p(:,2),h,nodes,'face');
u=(u*T)/n; v=(v*T)/n; %velocities are in km/yr
Dx =(alpha*abs(u))+De; Dy =(alpha*abs(v))+De;
S=sparse(nnodes,nnodes);
P=sparse(nnodes,nnodes);

for elem=1:nelem;
    i = nodes(elem,1); j = nodes(elem,2); k = nodes(elem,3);
    enodes=nodes(elem,:); % row of t = node numbers of the 3 corners of triangle e
    Pe=[ones(3,1),p(enodes,:)]; % 3 by 3 matrix with rows=[1 xcorner ycorner]
    delta=(abs(det(Pe))/2); % area of triangle (km^2) e = half of parallelogram area
    betai = nodey(j) - nodey(k);
    betaj = nodey(k) - nodey(i);
    betak = nodey(i) - nodey(j);
    gammai = nodex(k) - nodex(j);
    gammaj = nodex(i) - nodex(k);
    gammak = nodex(j) - nodex(i);

%ADVECTION
S(i,i) = S(i,i) + u(elem)*betai/6 + v(elem)*gammai/6;
S(i,j) = S(i,j) + u(elem)*betai/6 + v(elem)*gammai/6;
S(i,k) = S(i,k) + u(elem)*betai/6 + v(elem)*gammai/6;
S(j,i) = S(j,i) + u(elem)*betaj/6 + v(elem)*gammaj/6;
S(j,j) = S(j,j) + u(elem)*betaj/6 + v(elem)*gammaj/6;
S(j,k) = S(j,k) + u(elem)*betaj/6 + v(elem)*gammaj/6;
S(k,i) = S(k,i) + u(elem)*betak/6 + v(elem)*gammak/6;
S(k,j) = S(k,j) + u(elem)*betak/6 + v(elem)*gammak/6;
S(k,k) = S(k,k) + u(elem)*betak/6 + v(elem)*gammak/6;


%DISPERSION
S(i,i) = S(i,i) + Dx(elem)*betai*betai/(4*delta) + Dy(elem)*gammai*gammai/(4*delta);
S(i,j) = S(i,j) + Dx(elem)*betai*betaj/(4*delta) + Dy(elem)*gammai*gammaj/(4*delta);
S(i,k) = S(i,k) + Dx(elem)*betai*betak/(4*delta) + Dy(elem)*gammai*gammak/(4*delta);
S(j,i) = S(j,i) + Dx(elem)*betaj*betai/(4*delta) + Dy(elem)*gammaj*gammai/(4*delta);
S(j,j) = S(j,j) + Dx(elem)*betaj*betaj/(4*delta) + Dy(elem)*gammaj*gammaj/(4*delta);
S(j,k) = S(j,k) + Dx(elem)*betaj*betak/(4*delta) + Dy(elem)*gammaj*gammak/(4*delta);
S(k,i) = S(k,i) + Dx(elem)*betak*betai/(4*delta) + Dy(elem)*gammak*gammai/(4*delta);
S(k,j) = S(k,j) + Dx(elem)*betak*betaj/(4*delta) + Dy(elem)*gammak*gammaj/(4*delta);
S(k,k) = S(k,k) + Dx(elem)*betak*betak/(4*delta) + Dy(elem)*gammak*gammak/(4*delta);

%TIME MATRIX
P(i,i)=4*delta/12;
P(j,j)=4*delta/12;
P(k,k)=4*delta/12;
```

```
end

%Below finds velocity components normal to boundaries
tn=topnodes;
bn=bnodes1;
ub=abs(T*hx/n); %magnitude for flux boundaries
vb=abs(T*hy/n); %magnitude for flux boundaries
%Find dx for boundaries
for i=1:length(bn)-1;
bn1dx(i)=p(bn(i),1)-p(bn(i+1),1);
end
bn1dx=[bn1dx mean(bn1dx)];

for i=1:length(tn)-1;
tndx(i)=p(tn(i),1)-p(tn(i+1),1);
end
tndx =[tndx mean(tndx)];

%Find dy for boundaries
for i=1:length(bn)-1;
bn1dy(i)=p(bn(i),2)-p(bn(i+1),2);
end
bn1dy=[bn1dy mean(bn1dy)];

for i=1:length(tn)-1;
tndy(i)=p(tn(i),2)-p(tn(i+1),2);
end
tndy=[tndy mean(tndy)];

%Find aquifer flux component normal to the boundary
for i=1:length(bn);
BV(i) = (((vb(bn(i)).^2+ub(bn(i)).^2)).^(1/2))*(3/2)*...
    cos(atan(((-bn1dx(i)/bn1dy(i))-(abs(vb(i))/ub(bn(i))))));
end

for i=1:length(tn);
TV(i) = (((vb(tn(i)).^2+ub(tn(i)).^2)).^(1/2))*(3/2)*...
    cos(atan(((-tndx(i)/tndy(i))-(abs(vb(i))/ub(tn(i))))));
end

%Distance of line segments between top nodes ~0.28
for i=1:length(tn)-1;
dtop(i)=pdist([p(tn(i),1) p(tn(i),2); p(tn(i+1),1) p(tn(i+1),2)]);
end
dtop = [dtop mean(dtop)];

%Distance of line segments between bottom nodes ~0.28
for i=1:length(bn)-1;
dbot(i)=pdist([p(bn(i),1) p(bn(i),2); p(bn(i+1),1) p(bn(i+1),2)]);
end
dbot = [dbot mean(dbot)];
```

```
%Below are the figure options

%Quiver plot of flow vectors
figure(2)
triquiver(t,p(:,1),p(:,2),hx,hy); axis image
set(gcf, 'color', 'w')
title('Head Gradient and Groundwater Flow Vectors')

%Surface plot of head gradients
figure(3)
hf=trimesh(t,p(:,1),p(:,2),h(:,:),'LineWidth',1.2,'Facecolor','interp');hold on
colormap('summer');
colorbar;
axis image; grid off; view(2);
set(gcf, 'color', 'w')
title('Head Gradient and Groundwater Flow Vectors')
axis([0 10 0 20 0 3]);
xlabel('Kilometers'); ylabel('Kilometers');zlabel('Head (Kilometers)');

EA=delta; %Element Area
EV=EA*b*n; %Element volume
RR=w; %recharge rate (km/yr)
rhs2 = zeros(nnodes,1);
alltime=0:dt:tend;
c_old=ones(nnodes,1)*c0;

for m=2:length(alltime);
K=alltime(m);
delta_t=alltime(m)-alltime(m-1);
F=S+(P*b/delta_t);
rhs2=P*b*c_old/delta_t;
rhs2(w_elem) = rhs2(w_elem) + ((cr-c_old(w_elem))*(RR*delta));
% rhs2(topnodes) = rhs2(topnodes) - (TV'.*dtop'.*c_old(topnodes));
rhs2(bnodes1) = rhs2(bnodes1) - (BV'.*dbot'.*c_old(bnodes1));

for i = 1:length(topnodes);
    rhs2(topnodes(i)) = c0; %conentration of top boundary
    F(topnodes(i),:) = zeros(1,nnodes);
    F(topnodes(i),topnodes(i)) = 1;
end

str=sprintf('Time yrs (%i)',K);

c=F\rhs2;
c_old=c;
end

%Surface plot of salinity concentrations
figure(4)
hf=trimesh(t,p(:,1),p(:,2),c,'LineWidth',0.1,'Facecolor','interp');hold on
```

```
colormap('jet');
colorbar;
caxis([0 c0]);
format shortG
title('Groundwater Salinity (mg/l) Change','fontweight','bold','fontsize',10);
[~]=textloc(str,3,[],[]);
set(gcf, 'color', 'w')
axis image; ylabel('KM & S/dm^{3}'), xlabel('KM');
axis off
grid off
xlim([1 10]);ylim([0 20]);
view(2);
set(gcf,'color','w','Position', [50 50 700 600]);
```

BIBLIOGRAPHY

Alam, K. M., S. Hasan, M. Khan, and J. Whitney (1990), Geological map of banlgadesh.

Alam, M. (1996), *Subsidence of the GangesBrahmaputra Delta of Bangladesh and Associated Drainage, Sedimentation and Salinity Problems*, 169–192 pp., Springer.

Alam, M. G. M., G. Allinson, F. Stagnitti, A. Tanaka, and M. Westbrooke (2002), Arsenic contamination in bangladesh groundwater: A major environmental and social disaster, *International Journal of Environmental Health Research*, *12*(3), 235–253.

Auerbach, L. E. W. (2013), In the balance: Natural vs. embanked landscapes on the ganges brahmaputra tidal delta plain, Master's thesis, Vanderbilt University.

Aziz, Z., A. Van Geen, M. Stute, R. Versteeg, A. Horneman, Y. Zheng, S. Goodbred, M. Steckler, B. Weinman, I. Gavrieli, et al. (2008), Impact of local recharge on arsenic concentrations in shallow aquifers inferred from the electromagnetic conductivity of soils in araihazar, bangladesh, *Water Resources Research*, *44*(7).

Bahar, M. M., and M. S. Reza (2010), Hydrochemical characteristics and quality assessment of shallow groundwater in a coastal area of southwest bangladesh, *Environmental Earth Sciences*, *61*(5), 1065–1073.

Brammer, H. (1983), Agriculture and food production in polder areas, *Water International*, *8*(2), 74–81.

Bronk, C., Ramsey (2013), Oxcal program v4.2.

Burgess, W. G., M. A. Hoque, H. A. Michael, C. I. Voss, G. N. Breit, and K. M. Ahmed (2010), Vulnerability of deep groundwater in the bengal aquifer system to contamination by arsenic, *Nature Geoscience*, *3*(2), 83–87.

Cook, P., and D. Solomon (1997), Recent advances in dating young groundwater: chlorofluorocarbons, 3H3He and 85Kr, *Journal of Hydrology*, *191*(14), 245–265.

Cook, P., G. Walker, and I. Jolly (1989), Spatial variability of groundwater recharge in a semiarid region, *Journal of Hydrology*, *111*(1), 195–212.

Cook, P., G. Walker, G. Buselli, I. Potts, and A. Dodds (1992), The application of electromagnetic techniques to groundwater recharge investigations, *Journal of Hydrology*, *130*(1), 201–229.

Davis, S. N., and R. J. M. DeWiest (1966), *Hydrogeology, 463*, John Wiley, New York.

Delsman, J., K. Hu-a ng, P. Vos, P. de Louw, G. Essink, P. Stuyfzand, and M. Bierkens (2013), Palaeo-modeling of coastal salt water intrusion during the holocene: an application to the netherlands., *Hydrology & Earth System Sciences Discussions*, *10*(11).

Essaid, H. (1986), A comparison of the coupled fresh water-salt water flow and the ghyben-herzberg sharp interface approaches to modeling of transient behavior in coastal aquifer systems, *Journal of Hydrology*, *86*(1), 169–193.

Evans, R., et al. (2001), Measuring the shallow porosity structure of sediments on the continental shelf: A comparison of an electromagnetic approach with cores and acoustic backscatter, *Journal of Geophysical Research: Oceans (1978–2012)*, *106*(C11), 27,047–27,060.

Farquharson, C. (2000), Background for program em1dfm, 1d modelling and inversion code for frequency domain measurements, *UBC-GIF (University of British Columbia-Geophysical Inversion Facility), Canada*.

George, G. (2013), Characterization of salinity sources in southwestern bangladesh evaluated through surface water and groundwater geochemical analyses, Master's thesis, Vanderbilt University.

Geyh, M. A., et al. (2000), An overview of^ 1^ 4c analysis in the study of groundwater, *Radiocarbon*, *42*(1), 99–114.

Goodbred, S. L., and S. A. Kuehl (2000), The significance of large sediment supply, active tectonism, and eustasy on margin sequence development: Late quaternary stratigraphy and evolution of the GangesBrahmaputra delta, *Sedimentary Geology*, *133*(3), 227–248.

Hoque, M., P. Ravenscroft, and K. Hassan (2003a), Investigation of groundwater salinity and gas problems in southeast bangladesh, *Groundwater resources and development in Bangladesh–background to the arsenic crisis, agricultural potential and the environment. Bangladesh Centre for Advanced Studies. University Press, Dhaka*.

Hoque, M., K. Hasan, and P. Ravenscroft (2003b), *Groundwater Resources and Development in Bangladesh*, 1ST ed., The University Press Ltd.

Hoque, M. A., and W. G. Burgess (2012), 14C dating of deep groundwater in the bengal aquifer system, bangladesh: implications for aquifer anisotropy, recharge sources and sustainability, *Journal of Hydrology*.

Hornberger, G., and P. Wiberg (2005), *Numerical Methods in the Hydrological Sciences*, 57, American Geophysical Union E-Text.

Huang, H., and I. Won (2000), Conductivity and susceptibility mapping using broadband electromagnetic sensors, *Journal of Environmental & Engineering Geophysics*, *5*(4), 31–41.

Khan, A. E., A. Ireson, S. Kovats, S. K. Mojumder, A. Khusru, A. Rahman, and P. Vineis (2011), Drinking water salinity and maternal health in coastal bangladesh: implications of climate change, *Environmental health perspectives*, *119*(9), 1328.

Kinniburgh, D., and P. Smedley (2001), Arsenic contamination of groundwater in bangladesh.

McArthur, J. M., P. Ravenscroft, S. Safiulla, and M. F. Thirlwall (2001), Arsenic in groundwater: testing pollution mechanisms for sedimentary aquifers in bangladesh, *Water Resources Research*, *37*(1), 109–117.

McNeill, J. (1996), *Why doesn't Geonics Limited build a multi-frequency EM31 or EM38?*, Geonics.

Michael, H. A., and C. I. Voss (2009), Estimation of regional-scale groundwater flow properties in the bengal basin of india and bangladesh, *Hydrogeology Journal*, *17*(6), 1329–1346.

Michael, H. A., C. J. Russoniello, and L. A. Byron (2013), Global assessment of vulnerability to sea-level rise in topography-limited and recharge-limited coastal groundwater systems, *Water Resources Research*, *49*(4), 2228–2240.

Morgan, J. P., and W. G. McIntire (1959), Quaternary geology of the bengal basin, east pakistan and india, *Geological Society of America Bulletin*, *70*(3), 319–342.

Motz, L. H. (1995), Discussion of a density-dependent flow and transport analysis of the effects of groundwater development in a freshwater lens of limited areal extent: the geneva area (florida, usa) case study, by panday et al.(1993), *Journal of contaminant hydrology*, *18*(4), 321–326.

MPO (1987), Groundwater resources of bangladesh. technical report nr 5, master plan organisation, dhaka, *Harza Engineering, USA, Mott MacDonald Ltd, UK, Meta Consultants, USA and EPC Ltd, Bangladesh.*

Mulligan, A. E., R. L. Evans, and D. Lizarralde (2007), The role of paleochannels in groundwater/seawater exchange, *Journal of Hydrology*, *335*(3), 313–329.

Ohio-Supreme-Court (1861), Frazier v. brown, dispute over groundwater usage.

Panday, S., P. S. Huyakorn, J. B. Robertson, and B. McGurk (1993), A density-dependent flow and transport analysis of the effects of groundwater development in a freshwater lens of limited areal extent: the geneva area (florida, usa) case study, *Journal of contaminant hydrology*, *12*(4), 329–354.

Persson, P.-O., and G. Strang (2004), A simple mesh generator in matlab, *SIAM review*, *46*(2), 329–345.

Plunkett, E. R. (1976), Handbook of industrial toxicology.

Rahman, M. A. T., R. K. Majumder, S. H. Rahman, and M. A. Halim (2011a), Sources of deep groundwater salinity in the southwestern zone of bangladesh, *Environmental Earth Sciences*, *63*(2), 363–373.

Rahman, M. A. T. M. T., R. K. Majumder, S. H. Rahman, and M. A. Halim (2011b), Sources of deep groundwater salinity in the southwestern zone of bangladesh, *Environmental Earth Sciences*, *63*(2), 363–373.

Rahman, M. M., M. Q. Hassan, M. S. Islam, and S. Shamsad (2000), Environmental impact assessment on water quality deterioration caused by the decreased ganges outflow and saline water intrusion in south-western bangladesh, *Environmental Geology*, *40*(1-2), 31–40.

Ramsey, C. B. (2009), Bayesian analysis of radiocarbon dates, *Radiocarbon*, *51*(1), 337–360.

Ravenscroft, P., W. G. Burgess, K. M. Ahmed, M. Burren, and J. Perrin (2005), Arsenic in groundwater of the bengal basin, bangladesh: Distribution, field relations, and hydrogeological setting, *Hydrogeology Journal*, *13*(5), 727–751.

Reimer, P. J., E. Bard, A. Bayliss, J. W. Beck, P. G. Blackwell, C. B. Ramsey, C. E. Buck, H. Cheng, R. L. Edwards, M. Friedrich, et al. (2013), Intcal13 and marine13 radiocarbon age calibration curves 0–50,000 years cal bp, *Radiocarbon*, *55*(4), 1869–1887.

Shamsudduha, M., R. G. Taylor, K. M. Ahmed, and A. Zahid (2011), The impact of intensive groundwater abstraction on recharge to a shallow regional aquifer system: evidence from bangladesh, *Hydrogeology Journal*, *19*(4), 901–916.

Small, C., and R. J. Nicholls (2003), A global analysis of human settlement in coastal zones, *Journal of Coastal Research*, pp. 584–599.

Smith, R. C., and D. B. Sjogren (2006), An evaluation of electrical resistivity imaging (eri) in quaternary sediments, southern alberta, canada, *Geosphere*, *2*(6), 287–298.

Syvitski, J. P., A. J. Kettner, I. Overeem, E. W. Hutton, M. T. Hannon, G. R. Brakenridge, J. Day, C. Vorosmarty, Y. Saito, L. Giosan, et al. (2009), Sinking deltas due to human activities, *Nature Geoscience*, *2*(10), 681–686.

Tasich, C., and G. Hornberger (2012), Effects of tidal fluctuations on a semi-confined aquifer system in southwest bangladesh, Master's thesis, Vanderbilt University.

Tran, L. T. (2012), Origin and extent of fresh groundwater, salty paleowaters and recent saltwater intrusions in red river flood plain aquifers, vietnam, *Hydrogeology journal*, *20*(7), 1295.

Triantafilis, J., and S. Lesch (2005), Mapping clay content variation using electromagnetic induction techniques, *Computers and Electronics in Agriculture*, *46*(1), 203–237.

Wang, Y., J. J. Jiao, J. A. Cherry, and C. M. Lee (2013), Contribution of the aquitard to the regional groundwater hydrochemistry of the underlying confined aquifer in the pearl river delta, china, *Science of The Total Environment*, *461462*, 663–671.

WARPO (2008–2009), National water management plan, *Water Resources Planning Organization: Annual Report*, *2008–2009*, 1–122.

Won, I. (2003), Small frequency-domain electromagnetic induction sensors: How in the world does a small broadband emi sensor with little or no source-receiver separation work?, *The Leading Edge*, *22*(4), 320–322.

Yu, W., C. Voss, H. Michael, F. L. Ahmed, K.M., M. Khan, and A. Tuinhof (2010), Implications of climate change for fresh groundwater resources in coastal aquifers in bangladesh, *Rep. of the World Bank, South Asia Reg*, *2010*, 105.

Zahid, A., M. Q. Hassan, K.-D. Balke, M. Flegr, and D. W. Clark (2008), Groundwater chemistry and occurrence of arsenic in the meghna floodplain aquifer, southeastern bangladesh, *Environmental geology*, *54*(6), 1247–1260.